

**Enhancement of R123
Pool Boiling by the
Addition of Hydrocarbons**

Mark A. Kedzierski

U.S. DEPARTMENT OF COMMERCE
Technology Administration
National Institute of Standards
and Technology
Building and Fire Research Laboratory
Gaithersburg, MD 20899

Enhancement of R123 Pool Boiling by the Addition of Hydrocarbons

Mark A. Kedzierski

U.S. DEPARTMENT OF COMMERCE
Technology Administration
National Institute of Standards
and Technology
Building and Fire Research Laboratory
Gaithersburg, MD 20899

October 1998



U.S. DEPARTMENT OF COMMERCE
William M. Daley, Secretary

TECHNOLOGY ADMINISTRATION
Gary R. Bachula, Acting Under Secretary
for Technology

NATIONAL INSTITUTE OF STANDARDS
AND TECHNOLOGY
Raymond G. Kammer, Director

U.S. DEPARTMENT OF ENERGY
Washington, D.C. 20858

ABSTRACT

This paper presents pool boiling heat transfer data for ten different R123/hydrocarbon mixtures. The data consisted of pool boiling performance of a GEWA-T™ surface for pure R123 and for ten dilute solutions of five different hydrocarbons: (1) pentane, (2) isopentane, (3) hexane, (4) cyclohexane, and (5) heptane with R123. The heat flux and the wall superheat were measured for each fluid at 277.6 K. A maximum (19 ± 3.5)% increase over the pure R123 heat flux was achieved with the addition of 0.5% mass isopentane to R123. Other mixtures of isopentane, pentane, hexane, and cyclohexane with R123 exhibited smaller maximums than that of the R123/isopentane (99.5/0.5) mixture. Presumably, a layer enriched in hydrocarbon at the heat transfer surface caused the heat transfer enhancement. Conversely, an R123/heptane (99.5/0.5) mixture and an R123/cyclohexane (99.5/0.5) mixture exhibited only degradations with respect to the pure component performance for all test conditions. Several characteristics of the hydrocarbons were examined to determine their influence on the boiling heat transfer performance: molecular weight, molecular structure, composition, surface tension, and vapor pressure.

Keywords: Additive, binary mixtures, enhanced heat transfer, fluid heating, GEWA-T™, hydrocarbons, pool boiling, R123, refrigerants, surfactant

INTRODUCTION

Typically, binary mixtures exhibit a boiling performance degradation compared to their pure components (Shock, 1982 and Thome, 1990). Yet, some special liquids, when added in small quantities, enhance the boiling performance of pure fluids. For the refrigeration and air-conditioning industry, a liquid additive would be an economical means of reducing manufacturing and/or operating costs. For example, a liquid additive for 1,1-dichloro-2,2,2-trifluoroethane (R123) would enable existing water chillers to operate more efficiently or enable new water chillers to meet the same duty with fewer tubes. Unfortunately, liquid additives that significantly enhance refrigerant boiling performance are rare.

Most of the work on liquid additives has been in surfactants for aqueous solutions (Jontz and Myers (1960), Shah and Darby (1973) and Wu et al. (1995)). Carey (1992) and Rosen (1978) describe how surfactants reduce the surface tension of water. Basically, the surfactant molecule must have polar and nonpolar ends, i.e., an amphipathic structure. The nonpolar end of the surfactant distorts the interior structure of the solution. The structural distortion allows a surfactant molecule to travel to the liquid-vapor interface with less work than is required to bring a water molecule to the surface. By definition, the surface tension of the liquid-vapor interface is lowered when less work is required to bring a molecule to the surface.

Not much research has been done on surfactants for refrigerants. Kedzierski (1999) measured a significant enhancement of R123 pool boiling with the addition of 1% and 2% hexane by mass to R123. He used the Gibbs adsorption equation and the Young and Dupre equation to speculate that the boiling heat transfer enhancement of R123 by the addition of hexane was caused by an accumulation of hydrocarbon at the boiling surface. In essence, the greater concentration of hydrocarbon or "excess layer" at the heat transfer surface caused a reduction of the surface energy between the solid surface and the liquid. The existence of an excess layer at the liquid-solid interface is analogous to the existence of a surfactant induced excess layer at a liquid-vapor interface. Consequently, the hydrocarbon is not a typical surfactant because it accumulates at the solid-liquid interface rather than the liquid-vapor interface. However, the reduction in the liquid-solid surface energy results in a similar reduction in bubble departure diameter that occurs with a conventional surfactant. As a consequence of the bubble size reduction, the active site density increases. A heat transfer enhancement existed when a favorable balance between an increase in site density and a reduction in bubble size occurs.

In the present study, five different hydrocarbons were tested as additives in various concentrations with R123 in an effort to investigate the enhancement mechanism of the excess layer. The various hydrocarbons were chosen for their wide range of properties: namely, normal boiling point, interfacial surface tension, molecular weight, and molecular structure. It was hypothesized that certain thermophysical and chemical properties of the hydrocarbon were favorable for the creation of an excess layer. For example, an R123/hydrocarbon mixture that behaved as an azeotrope in the bulk mixture would be more likely to exhibit a heat transfer enhancement with respect to pure R123. For an azeotropic mixture, the excess layer is formed due to the strong affinity of the hydrocarbon for the solid surface. Dilute solution of hydrocarbons with R123 and mixture of components with similar boiling points were unlikely to exhibit heat transfer degradations that can be associated with concentration gradients. It was also

believed that a large difference between the surface tension of the additive and the refrigerant would create a large potential to reduce the surface energy of the liquid-solid interface via the excess layer. The stability of the excess layer may rely on the molecular structure of the hydrocarbon. For example, a particular molecular structure of a hydrocarbon may be more conducive to the formation of an excess layer due to its degree of repulsion of the polar R123 molecules that are at the interface of the excess layer and the bulk liquid.

APPARATUS

Figure 1 shows a schematic of the apparatus that was used to measure the pool boiling data of this study. More specifically, the apparatus was used to measure the liquid saturation temperature (T_s), the average pool-boiling heat flux (q''), and the wall temperature (T_w) of the test surface at the root of the fin. The three principal components of the apparatus were test chamber, condenser, and purger. The internal dimensions of the test chamber were 25.4 mm \times 257 mm \times 1.54 m. The test chamber was charged with approximately 7 kg of R123 from the purger, giving a liquid height of approximately 80mm above the test surface. As shown in Fig. 1, the test section was visible through two opposing, flat 150 mm \times 200 mm quartz windows. The bottom of the test surface was heated with high velocity (2.5 m/s) water flow. The vapor produced by liquid boiling on the test surface was condensed by the brine-cooled, shell-and-tube condenser and returned as liquid to the pool by gravity.

To reduce the errors associated with the liquid saturation temperature measurement, the saturation temperature of the liquid was measured with two 450 mm long 1.6 mm diameter stainless steel sheathed thermocouples. The small diameter provided for a relatively rapid response time. Nearly the entire length of the thermocouple was in contact with either the test refrigerant vapor or liquid to minimize conduction errors. The tip of the two thermocouples were placed approximately 2 mm above and 150 mm (and 300 mm) to one side of the top of the test surface. This placement ensured that approximately 80 mm of the probe length was in relatively well-mixed liquid near the two-phase fluid above the test surface. To provide for a saturated liquid pool state, the mass of liquid in the pool was large compared to mass of liquid condensed. At the highest heat flux, it would require nearly one hour to evaporate and condense the entire test chamber charge. The lack of a temperature difference between the probe and the well-insulated, low emissivity, 38 mm aluminum test chamber walls essentially eliminated temperature errors due to radiation to the probe.

TEST SURFACE

Figure 2 shows the oxygen-free high-conductivity (OFHC) copper GEWA-TTM test plate used in this study. Commercially, flattening the tips of the GEWA-KTM surface forms the GEWA-TTM or "T-fin" surface. The GEWA-TTM surface in this study was machined directly onto the top of the test plate by electric discharge machining (EDM). Figure 3 shows a photograph of the fin surface. The gap between the fin-tips was 0.348 mm. The surface had approximately 667 fins per meter oriented along the short axis of the plate. The ratio of the surface area to the projected area of the surface was 2.47. The fin-tip width and the fin-height were 1.05 mm and 1.038 mm, respectively.

MEASUREMENTS AND UNCERTAINTIES

The standard uncertainty (u_i) is the positive square root of the estimated variance u_i^2 . The individual standard uncertainties are combined to obtain the expanded uncertainty (U). The expanded uncertainty is commonly referred to as the law of propagation of uncertainty with a coverage factor. All measurement uncertainties are reported for a 95% confidence interval.

The copper-constantan thermocouples and the data acquisition system were calibrated against a glass-rod standard platinum resistance thermometer (SPRT) and a reference voltage to a residual standard deviation of 0.005 K. The NIST Thermometry Group calibrated the fixed SPRT to two fixed points having expanded uncertainties of 0.06 mK and 0.38 mK. A quartz thermometer, which was calibrated with a distilled ice bath, agreed with the SPRT temperature to within approximately 0.003 K. Both the measured thermocouple electromotive force (EMF) and the measured 1 mV reference were regressed to the SPRT temperature. During a pool-boiling test, the 1 mV reference was measured prior to measuring each thermocouple EMF. The reference voltage was used to account for the drift in the acquisition measurement capabilities over time. Before each test run, the measurements of a thermocouple in the bath with the SPRT were compared. The mean absolute difference between the thermocouple and the SPRT was 0.06 K over one year. Considering the fluctuations in the saturation temperature during the test and the standard uncertainties in the calibration, the expanded uncertainty of the average saturation temperature was no greater than 0.04 K. Consequently, it is believed that the expanded uncertainty of the temperature measurements was less than 0.1 K. The saturation temperature was also obtained from a pressure transducer measurement with an uncertainty of less than 0.03 kPa. The uncertainty of the saturation temperature from a regression (with a residual standard deviation of 0.6 mK) of equilibrium data (Morrison and Ward, 1991) for R123 was 0.17 K. The saturation temperature obtained from the thermocouple and the pressure measurement nearly always agreed within ± 0.17 K for the pure R123 data.

Figure 2 shows the coordinate system for the 20 wells where individual thermocouples were force fitted into the side of the test plate. The wells were 16 mm deep to reduce conduction errors. Using a method given by Eckert and Goldstein (1976), errors due to heat conduction along the thermocouple leads were estimated to be well below 0.01 mK. The origin of the coordinate system was centered on the surface with respect to the y-direction at the root of the fin. Centering the origin in the y-direction improved the accuracy of the wall heat flux and temperature calculations by reducing the number of fitted constants involved in these calculations. The x-coordinate measures the distance normal to the heat transfer surface. The y-coordinate measures the distance perpendicular to the x-coordinate. The thermocouples were arranged in four sets of five aligned in the x-direction. Following a procedure given by Kedzierski and Worthington (1993), the size and arrangement of the thermocouple wells were designed to minimize the errors in the wall temperature and temperature gradient measurement.

The heat flux and the wall temperature were obtained by regressing the measured temperature distribution of the block to the governing two-dimensional conduction equation (Laplace equation). In other words, rather than using the boundary conditions to solve for the interior temperatures, the interior temperatures were used to solve for the boundary conditions following a backward stepwise procedure given in Kedzierski (1995).

A backward stepwise regression was used to determine the best model or the significant terms of the solution to the Laplace equation in rectangular coordinates for each data point. Most infinite series solutions should converge within nine terms. The backward stepwise method began by regressing the first nine terms of the Laplace infinite series solution to the twenty measured plate temperatures:

$$T = A_0 + A_1x + B_1y + A_2(x^2 - y^2) + 2B_2xy + A_3x(x^2 - 3y^2) + B_3y(3x^2 - y^2) + A_4(x^4 - 6x^2y^2 + y^4) + 4B_4(x^3y - xy^3) \quad 1$$

The above "full" model was reduced to its significant terms by removing terms with t-values less than two while maintaining the original residual standard deviation of the full model. Terms were removed one at a time. Regression of the 20 temperatures was done after each term with the smallest t-values was removed. Table 1 provides an overview of the various two-dimensional conduction models that were used to reduce the measured temperatures to heat fluxes and wall temperatures.

Fourier's law and the fitted constants (A_0, A_1, \dots, A_n) were used to calculate the average heat flux (q'') normal to and evaluated at the heat transfer surface as:

$$q'' = \left(\frac{1}{L_y} \int_{-\frac{L_y}{2}}^{\frac{L_y}{2}} k \frac{\partial T}{\partial x} dy \right)_{x=0} = \bar{k} A_1 \quad 2$$

where \bar{k} is the average thermal conductivity along the surface of the plate, and L_y is the length of the heat transfer surface as shown in Fig. 2.

The average wall temperature (T_w) was calculated by integrating the local wall temperature:

$$T_w = \left(\frac{1}{L_y} \int_{-\frac{L_y}{2}}^{\frac{L_y}{2}} T dy \right)_{x=0} = A_0 \quad 3$$

Siu et al. (1976) estimated the uncertainty in the thermal conductivity of OFHC copper to be about 2% to 3% by comparing round-robin experiments. Considering this, the relative expanded uncertainty in q'' was greatest at the lowest heat fluxes, approaching 10% of the measurement at 10 kw/m². In general, the $E_{q''}$ appears to be relatively constant between 6% and 3% for heat fluxes above 30,000 W/m². The average random error in the wall superheat -- ($\Delta T_s = \overline{T_w} - T_s$)-- was within 0.1 K. A more detailed discussion of the uncertainty analysis can be found in Kedzierski (1996). After the data was reduced, it was realized that only one of the two thermocouples used to measure the liquid saturation temperature was used to calculate the wall superheat. This oversight may have added approximately 0.05 K to the systematic error. Considering that the boiling curve may drift more than 0.05 K in a month due to surface aging,

the shift in superheat was considered to be inconsequential due to the comparative purpose of the study.

EXPERIMENTAL RESULTS

The heat flux was varied from 80 kW/m^2 to 10 kW/m^2 to simulate typical operating conditions of R123 chillers equipped with enhanced tubes. All pool boiling tests were taken at 277.6 K saturated conditions. The data were recorded consecutively starting at approximately 80 kW/m^2 and then descending to 10 kW/m^2 in intervals of approximately 4 kW/m^2 . The descending heat flux procedure minimized the possibility of any hysteresis effects on the data, which would have made the data sensitive to the initial operating conditions. Table 2 presents the measured heat flux and wall superheat for all of the data of this study. Table 3 gives the number of test days and data points for each fluid.

The mixtures were prepared by first charging approximately 90% of the R123 into the test chamber to a known mass. Next, measured weights of the particular spectrophotometric grade hydrocarbon were injected through a valve in the side of the test chamber (see Fig. 1). The liquid hydrocarbon was injected with a syringe through the valve, followed by flushing with the remaining R123 charge. The flushing of R123 through the valve and connecting tubes also assisted in mixing the charge. All compositions are determined from the masses of the charged components and are given on a mass percent basis. The maximum uncertainty of the composition measurement is approximately 0.02%, e.g. the range of a 0.5% composition is between 0.48% and 0.52%.

The pool boiling performance of dilute mixtures of R123 and the following hydrocarbons were measured at 0.5% and 1.0% by mass hydrocarbon: isopentane, pentane, hexane, and cyclohexane. An R123/isopentane (99.5/0.5) by mass mixture was also tested along with an R123/heptane (99.9/0.1) by mass mixture. Pure R123 pool boiling data was taken to provide a baseline for comparison to the mixtures.

Figures 4 through 14 are plots of the measured heat flux (q'') versus the measured wall superheat ($T_w - T_s$) for all of the fluids. On average, each fluid was tested over six days. For the most part, one day's test covered heat fluxes from 80 kW/m^2 to 10 kW/m^2 . The solid line is a cubic best-fit regression or estimated mean of the data. Two cubic fits were required to cover the low and the high heat flux data. Table 4 gives the constants for the cubic regression of the superheat versus the heat flux for each test fluid. The residual standard deviation of the regressions - representing the proximity of the data to the mean - are given in Table 5. On average, the residual standard deviation of the low heat flux and the high heat flux data about the mean is 0.17 K and 0.10 K, respectively. The dashed lines to either side of the mean represent the lower and upper 95% simultaneous (multiple-use) confidence intervals for the mean. The expanded uncertainty of the estimated mean wall superheat in the low heat flux region and the high heat flux region is approximately 0.1 K and 0.07 K, respectively. Table 6 provides the average mean wall uncertainty for low and high heat fluxes.

Figure 4 presents the boiling curve for pure R123 at 277.6 K on the GEWA-TTM surface. The boiling curve exhibits two characteristic regimes: a natural convection/boiling regime and a

vigorous nucleate boiling regime. The regimes are separated by the cessation of vigorous nucleate boiling (CVNB). The CVNB occurs for the pure R123 data at approximately 9.5 K (24 kW/m²). The nucleate boiling regime exists for superheats that are greater than the CVNB condition. Here, the heat transfer is governed primarily by the formation of isolated bubbles within the fin cavities. The superheats below the CVNB are insufficient to support vigorous bubble generation. Consequently, natural convection becomes a prevalent mode of heat transfer for superheats below CVNB. In this region, limited bubble activity exists.

Figure 4 compares the present R123 GEWA-T™ boiling curve to R123 GEWA-T™ boiling data that was taken approximately five years prior (Kedzierski, 1999) to the present data in the same apparatus and for the same surface. The data differ substantially in the vigorous boiling region, but agree closely in the natural convection/boiling region. Apparently, the surface condition has changed such that many nucleation sites have been eliminated. The surface was stored in a felt-lined wooden box for the years between testing. The surface was cleaned prior to installation in the test apparatus with acetone, Tarnex™, hot tap water, and acetone for both the 1993 and the present tests. Following the cleaning process, the surface was exposed to a heat lamp for several hours. Just prior to the present tests, the surface was used for active pool boiling testing for nearly two years after the storage period. Aging and/or fouling of the surface have produced an offset in the wall superheat of approximately 2 K. It is believed that the superheat offset is not caused by a malfunctioning of the test equipment because no equivalent offset between the measured saturation temperature and the saturation temperature obtained from the measured pressure was observed. Also, the agreement of low heat flux data for the two periods shows that the measurements are consistent. In addition, examination of the surface after the present tests revealed that it was fouled with a somewhat tacky substance. The surface may have been contaminated with decane from previous R123/decane pool boiling tests. The decane could have been adsorbed on the test surface in a manner similar to that, which was observed by Tamura et al. (1983) where surfactants were irreversibly adsorbed on metal surfaces.

Figure 4 also compares the NIST 1993 GEWA-T™ boiling curve to GEWA-TX™ boiling curve measured by Webb and Pais (1992) at equal saturation temperatures. The figure summarizes the geometrical differences between the plate tested in this study and the tube that Webb and Pais (1992) tested. The Webb and Pais (1992) GEWA-TX™ data agree with the 1993 data for heat fluxes above 64 kW/m² and at 10 kW/m² and is greater than the present data for intermediate heat fluxes. The maximum percent difference between the two data sets of 100% occurs at the CVNB.

The greater performance of the Webb and Pais (1992) GEWA-TX™ surface compared to the 1993 NIST data for the intermediate heat flux region was partly due to the greater fins-per-meter (fpm) and the additional notch enhancement of the GEWA-TX™ surface. Also, the gap between the fins (S_f) on the plate was significantly larger than that on the GEWA-TX™ tube. The smaller fin-gap and the notch are effective at enhancing heat transfer at low site densities. A narrower fin-gap encourages bubble coalescence within the cavity. The notch acts to increase the site density. As the site density increases with the heat flux and the surface becomes saturated with bubbles, these geometry effects become less effective at heat transfer enhancement. Also, a flat plate does not experience the convection, as reported by Cornwell and

Einarsson (1989), that is induced by bubbles that slide within the channels of the side of a tube. The sliding bubbles also act to seed upper portions of the tube with vapor. These mechanisms would be less influential at higher heat fluxes where most of the potential sites have become active with vigorous bubble activity. Consequently, the performance difference between the plate and the tube becomes less significant at larger heat fluxes.

Figure 4 also shows the predictions from a free convection correlation for a horizontal plate with the upper surface being heated which was recommended by Incropera and Dewitt (1985). Although the correlation is for a flat plate, it may be possible to account for the enhanced surface with the characteristic length defined as the surface area over the exterior perimeter of the plate. The predictions are substantially lower than the present measurements. This is consistent with the enhancement of the free convection by some nucleate boiling and the upward motion of bubbles.

Figures 5 through 14 show the boiling curve for each of the mixtures in this study. As was done for pure R123, the cubic regressions are shown as solid lines. Dotted lines depict the 95% simultaneous confidence intervals for the cubic fits. A cubic fit for the high and low heat flux regions were required for each mixture. The following discussion examines the relative heat transfer performance of the mixtures and that of pure R123.

Figures 15 through 20 illustrate the effect of the addition of the various hydrocarbons to R123 on heat transfer performance. The figures plot the ratio of the mixture to the pure R123 heat flux (q''_m/q''_p) versus the pure R123 heat flux (q''_p) at the same wall superheat. A heat transfer enhancement exists where the heat flux ratio is greater than one and the 95% simultaneous confidence intervals (depicted by shaded regions) do not include the value one.

Figure 15 shows that the R123/isopentane (99.5/0.5) mixture exhibits an enhancement for heat fluxes greater than approximately 24 kW/m^2 . The CVNB is located near 24 kW/m^2 . Consequently, the addition of isopentane to R123 improves the heat transfer associated with vigorous boiling more so than it does for low-active-site-density boiling region. The maximum heat flux ratio for the 99.5/0.5 mixture was 1.19 at 50 kW/m^2 . The average heat flux ratio for the R123/isopentane (99.5/0.5) mixture over the entire range of test heat fluxes was 1.10. The performance of the R123/isopentane (99/1) mixture is similar to that of the R123/isopentane (99.5/0.5) mixture but it has a higher uncertainty. The R123/isopentane (99.9/0.1) mixture shows a maximum near its CVNB and decreases for heat fluxes above the CVNB. For 99.5% confidence, no difference exists between the boiling performance of the 99.9/0.1 mixture and pure R123 for heat fluxes greater than 37 kW/m^2 .

Figure 16 shows that the R123/pentane (99.5/0.5) and (99/1) mixtures have similar heat flux ratio profiles. For example, both mixtures exhibit an enhancement for heat fluxes less than approximately 24 kW/m^2 and a degradation for heat fluxes greater than approximately 24 kW/m^2 . Consequently, the addition of pentane to R123 enhances the low-active-site-density region rather than the vigorous boiling region. The maximum heat flux ratio for the R123/pentane (99/1) mixture was 1.14 at 12.6 kW/m^2 . The average heat flux ratio for the R123/pentane (99/1) mixture over the entire range of test heat fluxes was 0.98. The

performance of the R123/pentane (99.5/0.5) mixture is similar to that of the R123/pentane (99/1) mixture but slightly less over nearly the entire heat flux range. The R123/pentane (99.5/0.5) mixture had a maximum heat flux ratio of 1.08 and an overall average heat flux ratio of 0.94.

Figure 17 shows the heat flux ratio for the R123/hexane (99.5/0.5) and R123/hexane (99/1) mixtures. The R123/hexane (99/1) mixture exhibits a maximum heat flux ratio of 1.13 in the low-active-site-density region at 24.4 kW/m^2 . Whereas, the R123/hexane (99.5/0.5) mixture exhibits a maximum heat flux ratio of 1.08 in the vigorous nucleate boiling region (41.8 kW/m^2). The average heat flux ratio for the entire test range was 1.04 and 1.01 for the R123/hexane (99.5/0.5) mixture and the R123/hexane (99/1) mixture, respectively. For 99.5% confidence, the R123/hexane (99.5/0.5) mixture boiling performance does not differ from that of pure R123 for heat fluxes greater than approximately 24 kW/m^2 .

Figure 18 shows data for an R123/hexane (99/1) mixture and an R123/hexane (98/2) mixture that were taken in 1993 (Kedzierski, 1999) on the same surface and the same apparatus that was used in the present study. The R123/hexane (99/1) mixtures for the present study and the 1993 study exhibit a maxima at the same heat flux. However, the magnitude of the heat flux ratio for the 1993 study is much greater than that of the present study. Recall that Fig. 4 showed that the pure R123 boiling curve of the 1993 study significantly differed in the high heat flux region from the previous study. Obviously, the surface characteristics of the GEWA-T™ test plate were altered in the five years between the 1993 study and the present study. Presumably, the surface characteristics play a role in determining the effectiveness of the hydrocarbon in enhancing the active site density for nucleate boiling. From this, it is suspected that the heat flux ratios presented in this study would not be universally applicable to other enhancement geometries.

Figure 19 shows that the addition of heptane by 5% mass to R123 causes a heat transfer degradation for heat fluxes from 15 kW/m^2 to 70 kW/m^2 . The maximum heat flux ratio for the R123/heptane (99.5/0.5) mixture is 0.94 and occurs at 17 kW/m^2 . The heat flux ratio steadily decreases with increasing heat flux to approximately 0.51 at 70 kW/m^2 .

Figure 20 shows the heat flux ratio for two mixtures of R123 and cyclohexane. The R123/cyclohexane (99.5/0.5) mixture exhibits a heat transfer degradation as compared to pure R123 for the entire heat flux range of the tests. The R123/cyclohexane (99/1) has nearly the same performance of the (99.5/0.5) mixture with the exception of a small enhancement ($q''_m/q''_p = 1.04$) at $q''_p = 21.7 \text{ kW/m}^2$.

ENHANCEMENT TRENDS

The following five parameters were investigated for their influence on the boiling heat transfer performance of the hydrocarbon/R123 mixture: (1) the molecular weight of the hydrocarbon; (2) the difference in the boiling points of pure components at 39.8 kPa ($T_h - T_p$); (3) the difference in surface tension between the hydrocarbon and R123 at 277.6 K ($\sigma_h - \sigma_p$); (4) the mixture composition; and (5) the molecular structure of the hydrocarbon. Presumably, these parameters govern the dynamics of the formation of the excess layer for the R123/hydrocarbon mixtures. The mixtures should behave azeotropically in the bulk mixture. For very dilute solutions, mixtures may have large difference in normal boiling points while still maintaining azeotropic

behavior (Lunger and Shealy, 1994). However, due to its affinity for the solid, the hydrocarbon comes out of solution to form a confined region of higher hydrocarbon concentration at the wall. The initial formation of the excess layer due to the affinity of the hydrocarbon for the solid surface causes a composition shift past the azeotropic composition that may further increase the excess concentration through preferential boiling of the refrigerant. In addition, the excess layer cannot form on the wall unless the surface tension of the hydrocarbon is greater than that of R123. Otherwise, the hydrocarbon will act as a surfactant by accumulating at the liquid-vapor interface.

In figures 21 through 26, a linear model was used to provide only an approximate description of the trends in the data. Consequently, nearly each plot contains one or two influential points (Belsley et al., 1980) that may be considered outliers for the linear model. Future research might focus on gathering more data to better describe these trends and to identify the cause of outliers from the apparent linear trends.

Figure 21 shows the heat flux ratio as a function of the molecular weight of the hydrocarbon in the R123/hydrocarbon mixture. In general, larger heat flux ratios are obtained for R123/hydrocarbon mixtures that have hydrocarbons with smaller molecular weights. Hydrocarbons with large molecular weights tend to “be sticky” or have a strong affinity for the solid surface. For this case, the thickness of the excess layer may act as fouling rather than a surfactant for the surface.

Also, Hydrocarbons with large molecular weights tend to have larger vapor pressures relative to R123. Figure 22 illustrates the same point with the difference in boiling points (at 277.6 K) rather than the molecular weight. An R123/hydrocarbon mixture with a large vapor pressure difference or difference in boiling points will more likely exhibit azeotropic behavior, which can lead to a degradation in the heat transfer (Kedzierski et al., 1992). For example, it is likely that the performance of the R123/heptane (99.5/0.5) mixture suffers due to concentration gradients in the liquid.

Figure 23 provides the heat flux ratio as a function of the difference between the surface tension of the pure hydrocarbon (σ_h) and that of the pure R123 (σ_p) at 277.6 K. The figure shows that larger heat flux ratios are associated with smaller differences in surface tension between the hydrocarbon and R123. For a binary mixture, an excess layer is a consequence of differences in surface tension between the component liquids. An additive becomes a liquid-vapor surfactant if its surface tension is less than that of the solute. For this case, the additive accumulates (forms an excess layer) at the liquid-vapor interface and lowers its surface tension. Conversely, if the surface tension of the additive is greater than that of the solute, the additive forms an excess layer at the solid-liquid interface. Here, the surface energy between the liquid and solid is reduced by the presence of the excess layer on the liquid-solid interface. Closer examination of Fig. 22 shows that isopentane may lower the surface tension of the liquid-vapor interface, while the other hydrocarbons may lower the surface tension of the liquid-solid interface. An excess layer at the liquid-vapor interface or one at the liquid-solid interface would produce the same result by different means. That is, a reduction in the surface-tension of either the liquid-vapor or the liquid-solid interface causes a reduction in the bubble contact angle which, in turn, can cause an

enhancement of the heat transfer (Kedzierski, 1999). Nevertheless, the difference between the surface tension of isopentane and R123 may be within the uncertainty of its prediction. Consequently, it is possible that all of the hydrocarbons act on the liquid-solid interface.

Figure 24 illustrates the influence of the molecular structure of the hydrocarbon on the heat flux ratio. Apparently, the structure of the hydrocarbon has little influence on the heat transfer performance of the mixture. There is insufficient data to substantiate that, in general, a branch-chain hydrocarbon will give the best heat transfer performance. Even though three different unbranched-chain hydrocarbons were tested, the data is inconclusive due to the divergence of the R123/heptane (99.5/0.5) data from the mean of the data. The molecular structure does not appear to be a primary factor in determining the influence of the additives on the R123 heat transfer performance.

Figures 25 and 26 show that neither the mole fraction nor the mass fraction have much influence on the heat transfer performance of the R123/hydrocarbon mixture. The slopes of the data appear to vary randomly from mixture to mixture. Consequently, each R123/hydrocarbon pair has a unique composition for optimum heat transfer performance.

CONCLUSIONS

The pool boiling performance of R123 on a GEWA-TTM surface was enhanced as much as (19% \pm 3%) by adding 0.5% mass isopentane. Overall, the R123/isopentane (99.5/0.5) mixture exhibited a 10 % heat transfer enhancement over the entire range of test heat fluxes. In addition, the R123/hexane (99.5/0.5) mixture showed an overall 4% and a maximum 13% heat transfer enhancement over pure R123. The pool boiling enhancement mechanism is presumably due to an accumulation of hydrocarbon at the boiling surface in the channels. Apparently, the excess layer reduces the surface-energy between the liquid and the heat transfer surface causing the production of small diameter bubbles. Smaller bubbles will induce higher site densities than larger bubbles. The site density is increased enough to more than compensate for the loss in bubble size and results in a net heat transfer enhancement.

The influence of several parameters on the pool boiling heat transfer of the R123/hydrocarbon mixtures was investigated. In general, larger heat flux ratios were obtained for R123/hydrocarbon mixtures than for hydrocarbons with smaller molecular weights. An R123/hydrocarbon mixture with a large difference in boiling points was more likely to exhibit azeotropic behavior, which led to a degradation in the heat transfer. Apparently, the structure of the hydrocarbon had little influence on the heat transfer performance of the mixture. Neither the mole fraction nor the mass fraction had much influence on the heat transfer performance of the R123/hydrocarbon mixture for the small composition range that was investigated.

ACKNOWLEDGEMENTS

This work was jointly funded by NIST and the U.S. Department of Energy (project no. DE-01-95CE23808.000 modification #A004) under Project Manager Esher Kweller. Thanks go to the following NIST personnel for their constructive criticism of the first draft of the manuscript: Dr. V. Payne, Mr. J. Gebbie, and Mrs. J. Land. The author would also like to express appreciation to

G. Glaeser and S. Nolan for data collection. Furthermore, the author extends appreciation to Dr. E. Lagergren for consultations on the uncertainty analysis.

NOMENCLATURE

English Symbols

A_s	actual surface area (m)
E_{T_w}	expanded uncertainty in the wall temperature (K)
$E_{q''}$	relative expanded uncertainty (%) in heat flux measurement
e	height of fin from tip to root (m)
k	thermal conductivity (W/m·K)
L_y	length of test surface (m)
p	exterior perimeter of test surface (m)
q''	average wall heat flux (W/m ²)
Ra_L	Rayleigh number based on A_s/p
r_c	radius of cavity mouth (m)
S_f	spacing or gap between fin-tips (m)
s	estimate of standard deviation
T	temperature (K)
T_w	temperature of surface at root of fin (K)
U	expanded uncertainty
u_i	standard uncertainty
x	test surface coordinate, Fig. 2 (m)
y	test surface coordinate, Fig. 2 (m)

Greek symbols

ΔT	wall superheat: $T_w - T_s$, (K)
σ	surface-tension (kg/s ²)

Subscripts

h	hydrocarbon
l	liquid
m	mixture
p	pure R123
s	saturated state, solid surface
v	vapor

Superscripts

-	average
---	---------

REFERENCES

- Carey, V. P., 1992, Liquid-Vapor Phase-Change Phenomena, Hemisphere, Washington.
- Cornwell, K., and Einarsson, J. G., 1989, "The Influence of Fluid Flow on Nucleate Boiling from a Tube," Eurotherm Seminar No. 8, Advances in Pool Boiling Heat Transfer, Paderborn, FRG, May 11-12, pp. 28-41.
- Belsley, D. A., Kuh, E., and Welsch, R. E., 1980, Regression Diagnostics: Identifying Influential Data and Sources of Collinearity, New York: Wiley.
- Eckert, E. R. G., and Goldstein, R. J., 1976, Measurements in Heat Transfer, Hemisphere, Washington, 2nd ed., pp. 9-11.
- Incropera, F. P., and DeWitt, D. P., 1985, Fundamentals of Heat and Mass Transfer, 2nd ed., John Wiley & Sons, New York, p. 439.
- Jontz, P. D., and Myers, J. E., 1960, "The Effect of Dynamic Surface Tension on Nucleate Boiling Coefficients," AIChE Journal, Vol. 6, No. 1. pp. 34-38.
- Kedzierski, M. A., Kim, J. H., and Didion, D. A., 1992, "Causes of the Apparent Heat Transfer Degradation for Refrigerant Mixtures," in *Two-Phase Flow and Heat Transfer*, HTD-Vol. 197, J. H. Kim, R. A. Nelson, and A. Hashemi, Eds., ASME, New York, pp. 149-158.
- Kedzierski, M. A., 1999, "Enhancement of R123 Pool Boiling by the Addition of N-Hexane," Journal of Enhanced Heat Transfer, Vol. 6, No. 4.
- Kedzierski, M. A., 1996, "Enhancement of R123 Pool Boiling by the Addition of N-Hexane," NISTIR 5780, U.S. Department of Commerce, Washington.
- Kedzierski, M. A., 1995, "Calorimetric and Visual Measurements of R123 Pool Boiling on Four Enhanced Surfaces," NISTIR 5732, U.S. Department of Commerce, Washington.
- Kedzierski, M. A., and Worthington, J. L. III, 1993, "Design and Machining of Copper Specimens with Micro Holes for Accurate Heat Transfer Measurements," Experimental Heat Transfer, Vol. 6. pp. 329-344.
- Lunger, B. S., and Shealy, G. S., 1994, "Compositions of a Hydrofluorocarbon and a Hydrocarbon," International Patent WO 94/18282.
- Morrison, G, and Ward, D. K., 1991, "Thermodynamic Properties of Two Alternative Refrigerants: 1,1-Dichloro-2,2,2-Trifluoroethane (R123) and 1,1,1,2-Tetrafluoroethane (R134a)," Fluid Phase Equilibria, Vol. 62, pp. 65-86.
- Rosen, M. J., 1978, Surfactants and Interfacial Phenomena, John Wiley & Sons, New York, p.57.

Shah, B. H., and Darby, R., 1973, "The Effect of Surfactant on Evaporative Heat Transfer in Vertical Film Flow," Int. J. Heat Mass Transfer, Vol. 16, pp. 1889-1903.

Shock, R. A. W., 1982, "Boiling in Multicomponent Fluids," Multiphase Science and Technology, Hemisphere Publishing Corp., Vol. 1, pp. 281-386.

Siu, M. C. I., Carroll, W. L., and Watson, T. W., 1976, "Thermal Conductivity and Electrical Resistivity of Six Copper-Base Alloys," NBSIR 76-1003, U.S. Department of Commerce, Washington.

Tamura, J., Tse, J. T., and Adamson, A. W., 1983, J. Japan Petrol. Inst. Vol. 26, p. 309.

Thome, J. R., 1990, Enhanced Boiling Heat Transfer, Hemisphere Publishing Corp., New York, Chap. 9.

Webb, R.L., and Pais, C., 1992, "Nucleate Pool Boiling Data for Five Refrigerants on Plain, Integral-fin and Enhanced Tube Geometries," Int. J. Heat Mass Transfer, Vol. 35, No. 8, pp. 1893-1904.

Wu, W., Yang, Y., and Maa, J., 1995, "Enhancement of Nucleate Boiling Heat Transfer and Depression of Surface Tension by Surfactant Additives," J. Heat Transfer, Vol. 117, pp. 526-529.

Table 1 Conduction model choice

Fluid	$X_0 = \text{constant (all models)}$ $X_5 = y(3x^2 - y^2)$		$X_1 = x$ $X_6 = x(3y^2 - x^2)$	$X_2 = y$ $X_7 = x^4 + y^4 - 6(x^2)y^2$	$X_3 = xy$ $X_8 = yx^3 - xy^3$	$X_4 = x^2 - y^2$
	Low q''	High q''				
R123/isopentane (99.9/0.1)	X_1, X_6, X_7 (5 of 17) 29% X_1, X_2, X_3 (4 of 17) 24% X_1, X_2 (3 of 17) 18%	X_1, X_6, X_7 (5 of 17) 29% X_1, X_2, X_3 (4 of 17) 24% X_1, X_2 (3 of 17) 18%				
R123/isopentane (99.5/0.5)	X_1 (3 of 13) 23% X_1, X_6, X_7 (2 of 13) 15%	X_1, X_3, X_6, X_7 (43 of 117) 37% X_1, X_3, X_4, X_7 (25 of 117) 21% X_1, X_5, X_6, X_7 (13 of 117) 11%				
R123/isopentane (99/1)	X_1, X_3, X_6, X_7 (25 of 64) 39% X_1, X_4, X_5, X_7 (12 of 64) 19% X_1, X_3, X_4, X_7 (6 of 64) 9%	X_1, X_3, X_6, X_7 (25 of 64) 39% X_1, X_4, X_5, X_7 (12 of 64) 19% X_1, X_3, X_4, X_7 (6 of 64) 9%				
R123/pentane (99.5/0.5)	X_1 (11 of 52) 21% X_1, X_5, X_6, X_7 (10 of 52) 19% X_1, X_6, X_7 (8 of 52) 15%	X_1 (11 of 52) 21% X_1, X_5, X_6, X_7 (10 of 52) 19% X_1, X_6, X_7 (8 of 52) 15%				
R123/pentane (99/1)	X_1 (6 of 43) 14% X_1, X_5, X_6, X_7 (6 of 43) 14% X_1, X_2, X_6, X_7 (6 of 43) 14%	X_1, X_2, X_6, X_7 (33 of 70) 47% X_1, X_2, X_4, X_7 (9 of 70) 13% X_1, X_4, X_5, X_7 (8 of 70) 11%				
R123/hexane (99.5/0.5)	X_1, X_5, X_6, X_7 (10 of 49) 20% X_1, X_3, X_6, X_7 (7 of 49) 14% X_1, X_3 (8 of 49) 16%	X_1, X_3, X_4, X_7 (30 of 118) 25% X_1, X_3, X_6, X_7 (28 of 118) 24% X_1, X_2, X_6, X_7 (28 of 118) 16%				
R123/hexane (99/1)	X_1, X_3, X_6, X_7 (26 of 110) 24% X_1, X_2, X_6, X_7 (18 of 110) 16% X_1, X_3, X_4, X_7 (17 of 110) 15%	X_1, X_3, X_6, X_7 (26 of 110) 24% X_1, X_2, X_6, X_7 (18 of 110) 16% X_1, X_3, X_4, X_7 (17 of 110) 15%				
R123/heptane (99.5/0.5)	X_1 (12 of 33) 36% X_1, X_3 (9 of 33) 27% X_1, X_6, X_7 (4 of 33) 12%	X_1, X_3, X_6, X_7 (47 of 78) 60% X_1, X_3, X_4, X_7 (27 of 78) 35% X_1, X_2, X_4, X_7 (2 of 78) 3%				
R123/cyclohexane (99.5/0.5)	X_1, X_2, X_3 (11 of 38) 29% X_1, X_2, X_3, X_6 (5 of 38) 13% X_1, X_2, X_4, X_5 (4 of 38) 11%	X_1, X_3, X_6, X_7 (43 of 181) 24% X_1, X_4, X_5, X_7 (34 of 181) 19% X_1, X_2, X_4, X_7 (14 of 181) 8%				
R123/cyclohexane (99/1)	X_1, X_3, X_6, X_7 (38 of 124) 31% X_1, X_3, X_4, X_7 (23 of 124) 19% X_1, X_3, X_4, X_6 (9 of 124) 7%	X_1, X_3, X_6, X_7 (38 of 124) 31% X_1, X_3, X_4, X_7 (23 of 124) 19% X_1, X_3, X_4, X_6 (9 of 124) 7%				
R123	X_1, X_5, X_6, X_7 (23 of 66) 35% X_1, X_6, X_7 (14 of 66) 21% X_1, X_3, X_6, X_7 (7 of 66) 11%	X_1, X_3, X_6, X_7 (57 of 210) 27% X_1, X_3, X_4, X_7 (52 of 210) 25% X_1, X_2, X_6, X_7 (34 of 210) 16%				

Table 2 Pool boiling data

R123/hexane (99.5/0.5) File: GT5HEX.DAT		R123/hexane (99/1) File: GT1HEX.DAT		R123/isopentane (99.5/0.5) File: GTSISO.DAT		R123/isopentane (99/1)	
$\Delta T_s(K)$	$q'' (W/m^2)$	$\Delta T_s(K)$	$q'' (W/m^2)$	$\Delta T_s(K)$	$q'' (W/m^2)$	$\Delta T_s(K)$	$q'' (W/m^2)$
10.604	76976.3	10.553	77774.6	10.654	84348.5	9.784	41637.8
10.623	76334.3	10.551	78431.4	10.640	84685.0	9.583	33724.6
10.611	76623.8	10.530	78414.9	10.638	85543.1	9.529	34904.6
10.529	68496.7	10.196	54406.1	10.452	73786.4	9.531	34502.4
10.519	68946.4	10.185	53758.2	10.427	73821.7	9.565	32421.6
10.347	58373.2	10.182	53198.0	10.426	73631.0	9.515	32173.3
10.398	55786.1	9.986	44074.9	10.246	64881.1	9.501	31459.9
10.383	55593.8	9.962	44109.0	10.201	64339.2	8.937	23012.7
10.113	47180.3	9.935	43432.2	10.195	63898.0	8.916	22590.1
10.092	46989.9	9.778	35491.8	10.007	51668.5	8.164	10286.3
10.016	42193.1	9.808	35864.8	9.944	53399.3	6.147	10606.9
10.000	41713.3	9.698	36474.9	9.978	52060.0	6.109	10469.0
10.004	42045.1	9.199	27075.3	9.978	52060.0	6.159	7894.2
9.933	36958.1	9.183	27380.7	9.944	53399.3	6.147	7767.0
9.897	38522.3	9.256	26730.7	9.935	53777.2	6.109	7822.5
9.894	39932.8	8.148	19796.7	9.929	54201.9	6.147	6856.1
9.653	30721.0	8.145	20281.5	9.929	54201.9	6.109	6856.1
9.627	31256.0	6.933	14662.9	9.929	54201.9	6.109	6856.1
9.666	30996.2	7.017	14157.8	9.929	54201.9	6.109	6856.1
9.292	25087.9	7.086	14553.1	9.929	54201.9	6.109	6856.1
9.287	24930.5	6.121	13214.8	9.929	54201.9	6.109	6856.1
9.316	25257.3	6.072	12567.3	9.929	54201.9	6.109	6856.1
9.136	24815.3			9.929	54201.9	6.109	6856.1
8.465	20630.1			9.929	54201.9	6.109	6856.1
8.574	20612.2			9.929	54201.9	6.109	6856.1
8.560	20257.6			9.929	54201.9	6.109	6856.1
10.604	75278.3			9.929	54201.9	6.109	6856.1
10.587	75395.3			9.929	54201.9	6.109	6856.1
10.586	74754.7			9.929	54201.9	6.109	6856.1
10.428	61473.8			9.929	54201.9	6.109	6856.1
10.433	61547.8			9.929	54201.9	6.109	6856.1
10.420	61182.4			9.929	54201.9	6.109	6856.1
10.328	51877.0			9.929	54201.9	6.109	6856.1
10.265	53048.0			9.929	54201.9	6.109	6856.1
10.252	53354.3			9.929	54201.9	6.109	6856.1
10.090	44846.0			9.929	54201.9	6.109	6856.1
10.000	41778.8			9.929	54201.9	6.109	6856.1
9.993	42878.2			9.929	54201.9	6.109	6856.1
9.907	39062.6			9.929	54201.9	6.109	6856.1
9.883	39467.7			9.929	54201.9	6.109	6856.1
9.884	39140.8			9.929	54201.9	6.109	6856.1
9.754	34072.1			9.929	54201.9	6.109	6856.1
9.751	34446.7			9.929	54201.9	6.109	6856.1
9.755	34102.5			9.929	54201.9	6.109	6856.1
9.494	28812.5			9.929	54201.9	6.109	6856.1
9.512	28807.3			9.929	54201.9	6.109	6856.1
9.493	29981.7			9.929	54201.9	6.109	6856.1
8.779	23280.0			9.929	54201.9	6.109	6856.1
8.740	23024.0			9.929	54201.9	6.109	6856.1
8.740	23339.3			9.929	54201.9	6.109	6856.1
8.023	17827.2			9.929	54201.9	6.109	6856.1
7.900	17413.7			9.929	54201.9	6.109	6856.1
7.942	17746.7			9.929	54201.9	6.109	6856.1
6.492	14171.2			9.929	54201.9	6.109	6856.1
6.428	13836.7			9.929	54201.9	6.109	6856.1
6.462	14062.6			9.929	54201.9	6.109	6856.1
3.218	4741.1			9.929	54201.9	6.109	6856.1
3.117	4574.3			9.929	54201.9	6.109	6856.1
3.117	4420.8			9.929	54201.9	6.109	6856.1
10.654	75388.5			9.929	54201.9	6.109	6856.1
10.617	75022.5			9.929	54201.9	6.109	6856.1
10.591	75015.2			9.929	54201.9	6.109	6856.1
10.539	69794.5			9.929	54201.9	6.109	6856.1
10.529	69862.0			9.929	54201.9	6.109	6856.1
10.516	69863.8			9.929	54201.9	6.109	6856.1
10.467	64970.8			9.929	54201.9	6.109	6856.1
10.465	65699.3			9.929	54201.9	6.109	6856.1
10.457	66477.8			9.929	54201.9	6.109	6856.1
10.343	59049.8			9.929	54201.9	6.109	6856.1
10.364	59818.4			9.929	54201.9	6.109	6856.1
10.365	59466.4			9.929	54201.9	6.109	6856.1
10.196	54406.1			9.929	54201.9	6.109	6856.1
10.185	53758.2			9.929	54201.9	6.109	6856.1
10.182	53198.0			9.929	54201.9	6.109	6856.1
9.986	44074.9			9.929	54201.9	6.109	6856.1
9.962	44109.0			9.929	54201.9	6.109	6856.1
9.935	43432.2			9.929	54201.9	6.109	6856.1
9.778	35491.8			9.929	54201.9	6.109	6856.1
9.808	35864.8			9.929	54201.9	6.109	6856.1
9.698	36474.9			9.929	54201.9	6.109	6856.1
9.199	27075.3			9.929	54201.9	6.109	6856.1
9.183	27380.7			9.929	54201.9	6.109	6856.1
9.256	26730.7			9.929	54201.9	6.109	6856.1
8.132	19483.4			9.929	54201.9	6.109	6856.1
8.148	19796.7			9.929	54201.9	6.109	6856.1
8.145	20281.5			9.929	54201.9	6.109	6856.1
6.933	14662.9			9.929	54201.9	6.109	6856.1
7.017	14157.8			9.929	54201.9	6.109	6856.1
7.086	14553.1			9.929	54201.9	6.109	6856.1
6.121	13214.8			9.929	54201.9	6.109	6856.1
6.072	12567.3			9.929	54201.9	6.109	6856.1
10.570	76641.4	8.739	76641.4	9.770	35075.1	9.784	41637.8
10.578	78231.7	10.657	78231.7	9.563	29471.4	9.583	33724.6
10.580	77518.1	10.653	77518.1	9.560	29997.0	9.529	34904.6
10.547	74399.2	10.656	74399.2	9.567	30191.8	9.531	34502.4
10.534	73565.2	10.524	67745.2	8.983	27705.0	9.565	32421.6
10.480	68138.2	10.521	67894.2	8.992	26041.7	9.515	32173.3
10.518	70904.3	10.542	66350.9	8.680	21257.7	9.501	31459.9
10.466	67804.6	10.457	62293.3	8.645	23278.6	8.937	23012.7
10.434	67040.6	10.311	62380.7	8.669	21631.0	8.916	22590.1
10.371	62251.6	10.163	57384.6	7.701	15876.2	6.164	10286.3
10.331	62257.4	10.145	58287.0	7.681	15840.2	6.147	10606.9
10.319	59935.1	10.136	56764.3	7.698	15593.3	6.109	10469.0
10.302	58019.1	10.040	49699.5	6.152	10927.9	10.559	7894.2
10.304	57738.0	10.053	50314.1	6.085	12517.2	10.540	7767.0
10.224	59335.5	10.062	50544.9	6.058	11953.4	10.631	7822.5
9.808	49379.3	9.897	40455.2	10.649	75537.2	10.456	6856.1
9.637	46088.8	9.860	41080.5	10.670	77683.7	10.417	68709.4
9.719	44248.0	9.848	40526.7	10.651	77426.8	10.414	67924.5
9.793	41833.5	9.608	34808.9	10.573	70097.6	10.284	59693.2
9.700	40135.5	9.708	35738.3	10.567	68973.5	10.238	58544.5
9.692	39575.4	9.697	35456.3	10.573	70444.8	10.224	59185.7
9.674	39495.1	9.405	30391.4	10.433	62357.0	10.120	48718.9
9.436	31964.9	9.417	29306.2	10.432	62290.6	10.129	48177.6
9.486	32283.2	9.336	33405.9	10.406	61760.1	10.123	48521.4
9.459	32134.6	9.186	28170.0	10.383	58079.8	10.000	42248.0
8.864	25410.7	9.178	31159.7	10.368	58048.6	9.930	44169.8
9.042	27275.5	9.239	28362.7	10.370	58455.2	9.966	43429.2
9.074	27578.6	9.084	26940.8	10.025	45078.1	9.706	33561.6
8.251	18885.6	9.114	26956.9	10.048	46033.3	9.692	33940.3
8.172	18909.1	9.109	29516.6	10.057	46645.7	9.685	34462.4
8.137	18794.3	8.628	18741.4	9.884	40089.1	9.303	25548.9
6.436	13780.7	8.656	20007.6	9.881	40019.9	9.313	25739.0
8.439	13333.7	8.684	20197.8	9.845	40327.2	9.267	25701.1
8.451	13317.0	10.742	79637.5	9.552	28680.9	9.027	24210.0
10.570	76641.4	10.742	80808.5	9.500	31137.1	9.004	24806.9
10.578	75278.3	10.714	80823.2	9.554	30300.0	9.016	24109.8
10.580	77518.1	10.590	72530.6	8.741	26801.8	8.401	18583.8
10.547	74399.2	10.583	72218.0	8.754	26030.5	8.429	18796.2
10.534	73565.2	10.566	71926.0	8.758	26630.3	8.429	18899.4
10.480	68138.2	10.406	59150.8	8.784	26480.1	3.392	3678.5
10.518	70904.3	10.378	57970.8	8.766	26027.0	3.379	3860.0
10.466	67804.6	10.381	59198.7	8.747	25919.4	3.552	4688.1
10.434	67040.6	10.375	54836.2	8.698	22920.2	10.529	80676.3
10.434	67040.6	10.388	54898.4	8.689	23038.0	10.538	84209.2
10.371	62251.6	10.380	54456.3	8.698	23453.7	10.577	84774.8
10.331	62257.4	10.072	42847.9	8.435	19934.3	10.287	62766.7
10.319	59935.1	10.116	46297.3	8.406	19199.2	10.254	61362.0
10.302	58019.1	10.202	47098.5	8.4			

File:
GT1ISO.DAT

$\Delta T, (K)$	$q'' (W/m^2)$
10.352	71133.9
10.354	70977.8
10.365	70357.8
10.287	62609.9
10.308	62244.9
10.320	62325.0
10.228	57487.2
10.233	57989.1
10.228	57490.6
10.175	52879.2
10.164	54135.8
10.163	54175.3
10.015	50071.3
10.039	50343.4
10.022	47730.2
9.796	42607.6
9.823	43213.5
9.760	38097.8
9.782	38176.7
9.790	38190.3
9.569	33099.9
9.602	31847.5
9.614	32446.7
9.446	29197.2
9.426	29083.5
9.428	29294.8
9.305	25883.7
9.320	24726.5
9.327	25091.9
9.235	23449.8
9.207	23752.3
9.240	23692.8
10.459	72382.4
10.488	74603.4
10.492	76190.3
10.451	73153.6
10.452	74738.3
10.427	74431.3
10.299	64095.1
10.276	64317.1
10.281	63856.4
10.161	56018.4
10.194	57432.1
10.179	55851.3
10.082	50338.1
10.083	50182.6
10.083	50182.6
9.884	40452.7
9.861	42031.2
9.839	42120.2
9.703	34202.9
9.690	34355.4
9.692	34394.9
9.529	31597.1
9.496	31542.6
9.514	31541.1
8.965	27338.6
9.049	26906.6
8.749	24366.6
8.711	23708.2
8.689	23276.4
7.865	18765.7
7.965	20086.0
7.989	19927.2

R123/isopentane
(99.9/0.1)

File:
GT01ISO.DAT

$\Delta T, (K)$	$q'' (W/m^2)$
10.784	75064.9
10.767	75491.0
10.759	76299.8
10.640	65597.2
10.619	65959.5
10.811	65900.3
10.517	57560.4
10.507	57447.0
10.447	56734.4
10.307	48342.1
10.351	49184.7
10.022	38453.5
10.021	38945.9
10.001	38691.2
9.757	31696.3
9.642	33268.7
9.658	32474.0
9.724	33584.7
9.345	27583.7
9.364	27692.2
9.343	27406.7
8.697	22064.7
8.693	23388.2
8.698	23636.9
7.800	15469.0

7.765	71942.8
7.780	17362.5
7.238	15016.7
7.159	14851.8
7.171	14856.7
10.784	75064.9
10.767	75491.0
10.759	76299.8
10.640	65597.2
10.619	65959.5
10.811	65900.3
10.517	57560.4
10.507	57447.0
10.447	56734.4
10.307	48342.1
10.351	49184.7
10.022	38453.5
10.021	38945.9
10.001	38691.2
9.757	31696.3
9.642	33268.7
9.658	32474.0
9.724	33584.7
9.345	27583.7
9.345	27692.2
9.343	27406.7
8.697	22064.7
8.693	23388.2
8.698	23636.9
7.800	15469.0

17342.8	9.985
17362.5	9.688
15016.7	9.743
14851.8	9.345
14856.7	9.334
75064.9	9.351
75491.0	8.837
76299.8	8.838
65597.2	8.807
65959.5	7.810
65900.3	7.936
57560.4	7.928
57447.0	10.780
56734.4	10.793
48342.1	10.761
49184.7	10.671
38453.5	10.643
38945.9	10.667
38691.2	10.569
31696.3	10.573
33268.7	10.565
32474.0	10.239
33584.7	10.257
27583.7	10.270
27692.2	9.962
27406.7	9.936
22064.7	9.897
23388.2	9.764
23636.9	9.745
15469.0	8.695
17342.8	8.527
17362.5	8.780
15016.7	7.494
14851.8	7.561
14856.7	7.596
73987.5	10.596
74282.6	10.662
69019.0	10.617
69208.8	10.435
68756.2	10.407
65174.1	10.382
65379.7	10.230
65843.2	10.215
54739.5	10.191
55914.8	10.035
56701.2	10.011
48345.4	9.992
44931.6	9.580
45114.2	9.582
45817.2	9.583
32379.2	9.075
32742.6	9.061
32781.4	9.073
27097.3	8.344
25213.2	8.357
27553.8	8.381
21284.2	6.650
18728.8	6.502
75358.4	6.821
75891.4	
75832.8	
78035.7	
73119.9	
73173.7	
72916.0	
60107.0	
59834.2	
60248.8	
56839.5	
56424.9	
56190.0	
54584.4	
54644.0	
54368.4	
50789.5	
51396.0	
47830.0	
48394.3	
47463.7	
42972.5	
43061.2	
43637.6	
32040.6	
31911.1	
30343.1	
20178.8	
19281.0	
17703.7	
73622.6	
73694.8	
74076.7	
70144.1	
69749.1	
70103.0	
60384.4	
60419.2	
59624.3	
55133.0	
55774.4	
55896.1	
55874.6	
46949.0	
47080.6	

R123/cyclohexane
(99/1)

File:
GT1CYC.DAT

$\Delta T, (K)$	$q'' (W/m^2)$
11.111	73931.5
11.104	74433.5
11.109	74214.3
10.999	61268.9
10.891	63279.4
10.880	63596.2
10.698	51435.6
10.719	51685.2
10.520	43234.2
10.483	43106.8
10.513	43118.7
10.517	43395.2
10.093	35239.6
10.079	35348.9
9.378	29113.8
9.179	30040.6
9.186	29446.3
8.595	25827.3
8.631	24404.8
8.652	24281.4
8.752	23204.8
8.669	22277.0
7.446	16243.3
7.432	16333.9
7.464	16874.4
6.814	14341.8
6.750	13640.9
6.818	13683.9
11.052	72977.7
11.028	72986.1
10.993	73500.7
10.870	61429.0
10.868	62990.8

48550.2	10.864
41309.9	10.839
38944.2	10.811
31310.9	10.798
31305.6	10.737
31313.5	10.731
23699.8	10.679
24487.5	10.435
24844.9	10.401
20208.4	10.395
18377.6	10.168
18562.9	10.181
74295.0	10.098
74432.3	10.072
72649.3	10.099
70952.0	10.112
70865.0	9.784
70688.7	9.773
61430.3	9.763
61442.5	9.325
61338.5	9.351
51297.6	8.918
51977.8	8.919
52244.1	8.077
41686.0	8.233
41515.6	11.019
40585.4	11.018
36986.8	10.999
37402.2	10.939
25723.4	10.766
24261.1	10.746
23735.4	10.323
16355.0	10.308
16877.2	9.907
16709.5	9.953
74340.5	9.941
74664.6	9.051
74267.3	9.106
68088.6	8.970
67849.9	9.007
68048.1	8.913
56842.2	11.034
57715.8	11.034
57597.3	10.985
47870.0	10.958
47432.7	10.915
47393.0	10.883
36357.2	10.870
36053.8	10.753
36448.2	10.652
30827.9	10.668
30889.8	10.681
31004.1	10.558
21123.7	10.543
21082.4	10.573
21095.3	9.956
13227.1	10.079
12700.0	10.048
14151.4	9.609

10.864	62937.3
10.839	58121.0
10.811	57763.6
10.798	57966.7
10.737	54876.1
10.731	54279.6
10.679	51612.3
10.435	43853.9
10.401	43976.2
10.395	46224.5
10.168	37219.5
10.181	37183.8
10.098	36013.9
10.072	36433.3
10.099	36684.9
10.112	36468.9
9.784	30043.0
9.773	29914.4
9.763	29875.2
9.325	29422.4
9.351	29854.5
8.918	24778.9
8.919	24829.9
8.077	19621.8
8.233	18172.0
11.019	17527.0
11.018	75526.1
10.999	75553.5
10.939	72850.1
10.766	61456.5
10.746	62594.3
10.323	44437.2
10.308	43805.8
9.907	32811.2
9.953	33215.1
9.941	33256.8
9.051	24923.8
9.106	25346.3
8.970	22080.0
9.007	22367.5
8.913	23962.0
11.034	72713.3
11.034	72713.3
10.985	72498.7
10.958	71991.8
10.915	68456.1
10.883	68229.0
10.870	67813.6
10.753	63238.5
10.652	54786.4
10.668	56402.0
10.681	56147.3
10.558	52148.9
10.543	52429.4
10.573	52595.4
9.956	35129.9
10.079	34126.7
10.048	34802.8
9.609	28788.1
8.902	24190.0
8.911	23940.7
8.902	24142.6
7.772	16408.5
7.613	15951.8
7.595	16553.6
10.825	72928.5
10.897	78735.3
11.021	78846.7
10.848	71970.1
10.764	65598.4
10.654	59809.9
10.595	61058.2
10.561	60232.0
10.274	47316.7
10.263	47349.1
10.239	46464.3
10.131	42414.5
10.129	43668.3
10.151	44115.3
10.062	40621.1
9.852	36268.6
9.909	37081.8
9.924	37231.2
9.366	29054.2
9.361	29366.2
9.365	29224.1
9.139	25408.1
9.096	25090.0
9.092	25107.1
8.453	22173.6
8.460	22113.1
10.980	71766.3
10.984	71411.4
10.997	71826.8
10.965	67577.9
10.991	67793.3
10.943	68634.2
10.731	56275.7
10.706	56832.8
10.488	47339.9
10.496	47381.5
10.495	46853.0

62937.3	10.243
58121.0	10.249
57763.6	10.228
57966.7	9.967
54876.1	10.034
54279.6	10.053
51612.3	9.948
43853.9	9.677
43976.2	9.634
46224.5	9.398
37219.5	9.461
37183.8	9.026
36013.9	8.951
36433.3	8.907
36684.9	8.617

10.636	65833.4	10.928	75131.3	9.216	27545.1	10.572	69453.0	11.018	56155.390
10.637	66334.5	10.915	75925.2	9.475	26191.0	10.573	69418.7	11.013	56328.840
10.586	58678.1	10.678	61724.4	7.987	18726.0	10.590	69556.7	10.892	46680.610
10.572	56250.3	10.624	62145.0	7.985	18768.4	10.539	66985.0	10.886	48265.960
10.513	57677.0	10.597	62778.4	8.026	19215.9	10.539	66985.0	10.879	47013.360
10.464	50565.6	10.451	50695.5	6.618	13429.8	10.518	67281.8	10.635	38852.760
10.424	48328.5	10.434	50179.9	6.575	13439.0	10.521	66950.2	10.627	38025.290
10.383	51138.3	10.435	48968.8	6.547	13407.7	10.469	59108.2	10.647	38412.350
10.304	46753.4	10.436	46460.7	6.180	12348.1	10.549	71151.1	10.328	32643.710
10.291	46954.7	10.426	47625.1	6.121	13805.2	10.515	68719.6	10.325	32628.020
10.287	46596.9	10.410	49208.6	6.137	12091.4	10.512	70836.1	10.330	32425.280
10.008	34468.6	10.370	43418.1	5.711	11103.0	10.433	65771.5	9.747	29851.740
9.975	34410.7	10.362	44185.5	5.720	11336.2	10.451	65459.6	9.789	29929.970
9.998	33823.9	10.106	34834.5	5.736	11118.6	10.434	65215.2	9.766	29776.100
9.525	25780.3	10.052	33310.8	5.045	10170.3	10.365	57120.8	8.923	20076.290
9.482	25461.0	10.079	33951.9	5.030	10264.4	10.354	56416.4	8.901	21954.960
9.206	24545.0	9.656	30753.8	4.534	8660.2	10.366	56885.0	8.951	21850.880
9.039	23899.6	9.623	30566.4	4.477	8592.6	10.235	49449.2	8.462	17146.950
9.075	24279.5	9.751	31031.2	4.467	8609.4	10.184	50803.4	8.394	18648.020
8.652	22818.5	9.164	24618.7	3.939	6937.5	10.246	52638.6	8.386	18803.040
8.704	22186.8	9.133	24570.6	3.915	6915.5	10.111	45351.0	7.976	16675.900
8.676	22486.6	9.150	24352.2	3.912	6853.6	10.153	43431.7	7.896	16607.490
8.453	19270.4	9.705	32403.7	10.640	74426.3	10.091	45560.7	7.891	16583.510
8.359	20773.6	9.279	27905.8	10.642	74785.2	9.969	33820.4	11.224	76471.270
8.403	20816.7	8.978	21319.1	10.635	75207.8	9.922	33956.5	11.267	78175.070
6.506	13298.8	9.002	21752.8	10.612	72777.0	9.915	35022.5	11.277	78373.330
6.520	13287.5	9.001	21753.3	10.608	72351.7	9.543	26808.9	11.148	70748.320
6.576	13340.6	8.606	20838.2	10.600	72495.1	9.339	27086.7	11.158	70006.630
10.773	74484.0	8.617	20088.0	10.502	65423.9	9.282	26973.0	11.157	70063.700
10.749	72259.4	8.614	20226.1	10.485	65483.8	8.279	19779.7	10.988	60124.870
10.758	75320.7		10.483		64218.6	8.332	19835.4	10.961	60416.020
10.685	65898.5		10.313		47201.2	8.286	19489.5	10.960	61120.050
10.690	66033.3		10.285		47038.6	7.711	17895.6	10.744	51919.240
10.686	64801.7		10.231		47383.7	7.704	17286.2	10.716	54290.720
10.662	59741.6		10.070		39890.6	7.560	17017.9	11.382	72288.230
10.618	59501.1		10.065		39785.7	7.097	15874.4	11.389	72199.000
10.602	60409.5		10.095		40329.4	7.183	16058.6	11.368	71840.170
10.601	56648.2		9.818		27314.2	7.255	16214.1	11.271	64778.450
10.452	49822.4		9.821		27264.6	6.583	16049.0	11.279	64959.540
10.431	49130.6		9.789		27626.5	6.612	15928.3	11.258	64419.360
10.405	47988.8		8.878		26033.8	6.550	16078.1	11.208	60118.720
10.298	41881.2		8.873		26186.6	5.734	13160.1	11.180	60021.780
10.312	44029.1		8.887		24346.3	5.694	13039.3	11.158	60044.410
10.305	44707.4		8.503		21011.1	5.580	12579.6	10.970	53194.990
10.236	40406.8		8.513		20875.5	4.591	9225.9	10.981	53752.450
10.239	39927.7		8.492		21121.9	4.556	9401.8	11.047	53548.300
10.246	40099.6		7.741		19282.4	4.570	9381.3	10.693	42139.690
10.121	34616.8		7.647		19331.1	10.441	73523.3	10.756	42028.090
9.988	34660.5		7.8851.2	6.719	15784.9	10.450	73384.3	10.749	42120.740
9.942	33644.3		6.5946.5	6.792	16022.2	10.334	63502.7	10.548	34996.520
9.253	26161.4		6.5960.0	6.806	16159.7	10.300	63763.8	10.579	35532.950
9.263	25772.7		6.5402.3	6.217	14074.0	10.299	64051.4	10.554	35663.320
9.259	26310.2		5.1040.0	6.196	13969.4	10.125	48977.3	10.451	33308.550
11.079	73184.5		5.2760.9	6.214	13955.2	10.091	48079.3	10.451	33240.300
10.978	71583.3		5.5911.6	5.236	10568.5	10.110	46371.3	10.449	32831.390
10.944	71696.6		5.1735.6	5.439	11340.8	10.000	41144.6	10.228	30857.720
10.805	59297.2		5.1987.8	5.465	11488.4	9.975	40258.7	10.245	31168.600
10.745	60150.4		5.0154.4			9.981	40617.5	9.466	25534.810
10.783	58882.0		4.4844.2			9.793	31853.1	9.391	25713.020
10.623	53204.4		4.3849.3			9.799	31918.4	9.418	25642.390
10.585	52828.2		4.5196.8			9.796	32009.4	8.609	19153.960
10.504	43764.6		4.2984.1			8.806	21992.3	8.566	19518.790
10.483	44107.6		4.2021.2			8.831	22223.6	8.574	19426.800
10.293	35377.8		4.2167.6			8.836	22335.8	7.275	14814.380
10.305	36062.1		3.6777.8			8.073	18550.5	7.245	14792.260
10.301	36227.8		3.7931.3			8.039	20590.3	7.198	14791.260
9.481	27201.2		3.8756.1			8.062	18380.8	11.380	73828.450
9.510	24579.0		3.1528.8			6.540	15353.0	11.461	77214.940
9.563	24807.1		3.1656.4			6.497	15372.4	11.441	77833.630
10.908	75512.6		3.1816.9			6.481	15174.0	11.247	66935.390
10.877	75484.3		2.8344.5			5.983	13448.8	11.225	66874.650
10.897	75144.2		2.7753.0			5.896	13359.9	11.220	66113.950
10.809	66702.0		2.6931.0			5.480	11946.2	11.137	59114.020
10.806	66650.2		2.5133.2			5.477	11956.9	11.127	58760.120
10.787	66561.0		2.5503.5			5.128	10731.4	11.121	59234.130
10.739	62915.9		2.3343.2			5.210	11075.9	10.826	47345.450
10.739	62563.6		2.1465.8			4.418	8324.1	10.821	47688.610
10.730	62253.3		2.1550.9			4.448	8471.7	10.823	48001.470
10.475	51054.9		2.1461.4					10.508	38695.680
10.504	51292.7		1.6793.9					10.495	37150.810
10.525	51352.6		1.6919.3					10.028	29469.170
10.409	46063.0		1.6359.4					10.063	30036.540
10.406	45871.7		1.6338.8					10.050	30171.050
10.415	46551.3		1.6116.6					9.249	22354.330
10.283	40205.1		1.0593.9					9.274	22194.410
10.282	41321.0		1.0509.9					9.318	22598.170
10.276	40487.6		1.0496.6					8.979	20441.540
10.047	32725.6		1.0500.0					9.019	19213.640
10.005	32297.9		1.0420.0					8.944	21603.390
9.978	32298.2		1.0447.7					7.836	15999.110
9.451	26971.0		1.0445.5					7.821	15969.800
9.415	26625.1		1.0399.9					7.803	15912.550
9.343	25885.5		1.0408.8					7.202	13899.690
9.380	26111.9		1.0288.8					7.161	13709.550
9.374	26030.6		1.0266.6					7.123	13585.680
8.775	19639.9		1.0269.9						
8.737	19507.2		9.995						
8.725	20278.4		10.047						
7.954	16308.2		9.708						
8.020	16386.4		9.846						
8.011	16425.0		9.846						
10.920	74408.6		9.330						

R123/pentane
(99.5/0.5)
File:
GT5PEN.DAT

ΔT (K)	q'' (W/m ²)
10.530	77189.0
10.507	78270.7
10.531	78851.2
10.429	65946.5
10.440	65960.0
10.437	65402.3
10.311	51040.0
10.296	52760.9
10.352	55911.6
10.242	51735.6
10.238	51987.8
10.281	50154.4
10.113	44844.2
10.116	43849.3
10.140	45196.8
10.074	42984.1
10.074	42021.2
10.099	42167.6
10.005	36777.8
9.992	37931.3
9.976	38756.1
9.905	31528.8
9.939	31656.4
9.935	31816.9
9.772	28344.5
9.746	27753.0
9.684	26931.0
9.113	25133.2
9.142	25503.5
9.301	23343.2
8.636	21465.8
8.684	21550.9
8.647	21461.4
7.772	16793.9
7.823	16919.3
7.810	16359.4
10.638	77573.0
10.616	76419.1
10.593	75982.9
10.509	70652.4
10.496	70330.0
10.500	69908.5
10.420	60903.2
10.447	60664.5
10.445	60638.3
10.399	57382.0
10.408	57521.6
10.288	46924.1
10.266	46827.2
10.269	46581.0
9.995	34052.0
10.047	34344.9
9.708	26596.8
9.846	27419.1
9.846	26194.2
9.330	25167.9

R123/pentane
(99/1)
File:
GT1PEN.DAT

ΔT (K)	q'' (W/m ²)								
10.562	67849.5	9.158	24179.2	10.300	58432.3	10.491	84191.4	6.883	14027.3
10.546	70318.8	9.156	24096.8	10.081	50168.7	10.483	65151.8	6.765	13837.5
10.561	71190.3	9.161	24017.4	10.074	49677.1	10.388	55387.8	6.343	12681.1
10.505	65318.1	8.929	22063.2	10.074	49137.4	10.045	42880.3	6.423	12911.0
10.508	65563.0	8.918	21675.1	9.944	45286.3	10.112	46439.6	6.434	12901.3
10.489	65156.7	8.894	21962.9	9.925	45755.5	10.118	46352.3	5.723	11899.1
10.489	65156.7	10.642	74716.6	9.812	39678.3	9.990	40012.9	5.712	12018.3
10.429	58931.7	10.623	70798.8	9.803	39001.8	9.969	40055.1	5.718	12026.0
10.409	58934.5	10.602	71507.4	9.785	39460.0	9.935	37859.0	4.375	7998.6
10.406	58386.5	10.462	66053.5	9.653	30847.9	9.900	35900.8	4.319	7813.2
10.326	53430.4	10.546	70273.5	9.686	30830.0	9.905	35920.9	4.281	7743.2
10.319	53752.0	10.428	62980.0	9.666	31686.0	9.876	36314.4	4.063	74774.7
10.300	54158.8	10.403	62697.5	9.056	26718.1	9.643	30427.1	10.473	75828.3
10.156	50168.9	10.447	62857.3	9.057	26718.3	9.705	31029.8	10.476	75465.2
10.135	50253.9	10.357	55542.4	9.056	26923.7	9.603	28908.2	10.384	66881.8
9.916	39976.9	10.367	55176.5	8.103	20275.1	9.520	27983.9	10.379	67125.3
9.896	39837.1	10.229	55344.2	8.071	20061.4	9.526	27825.1	10.393	66602.5
9.900	39847.7	10.293	53744.1	10.565	74084.1	9.551	28000.5	10.309	58291.4
9.723	36242.7	10.170	46021.4	10.557	75398.2	9.370	29502.0	10.293	58641.1
9.740	36292.3	10.148	46255.9	10.576	77791.3	9.043	24847.9	10.155	53543.8
9.773	34923.3	10.125	46441.7	10.515	73731.3	9.031	23706.9	10.114	54085.5
9.527	30650.9	9.979	38281.9	10.536	73678.8	8.354	18301.1	10.127	53223.4
9.538	30498.3	9.993	39569.9	10.531	74241.4	8.418	18471.5	9.994	45418.1
9.584	29118.1	9.998	40472.2	10.393	61736.4	8.277	17623.9	9.978	44951.6
9.212	25495.8	9.906	37435.4	10.378	61166.2	6.601	12776.5	9.959	45357.5
9.133	26361.7	9.893	38141.4	10.361	58207.8	6.624	14208.8	9.827	37097.5
10.571	73561.9	9.903	37328.9	10.321	52763.1	10.533	76637.2	9.823	36973.2
10.614	77143.4	9.651	28001.7	10.319	54585.8	10.556	78693.5	9.825	37229.2
10.607	78115.3	9.625	28800.6	10.315	55210.8	10.558	79748.9	9.461	32987.3
10.546	70964.8	9.657	29526.1	10.170	45571.4	10.481	66708.8	8.401	32973.3
10.570	71110.9	9.341	28251.3	10.093	46878.7	10.427	66373.5	9.397	32954.7
10.566	71008.0	9.281	28307.2	10.103	47341.5	10.417	66810.2	9.021	28075.7
10.492	66332.9	9.068	28912.1	9.944	41402.8	10.337	60987.2	8.941	28929.1
10.479	64730.9	9.923	24843.4	9.923	40718.2	10.337	60987.2	9.027	28134.1
10.450	61133.5	9.092	24625.0	9.893	38389.6	10.317	60698.0	8.953	28435.7
10.440	61369.3	9.134	25838.8	9.706	32526.5	10.322	62050.1	8.985	29839.6
10.455	61404.8	8.843	20998.5	9.696	31833.2	10.175	52777.2	9.052	27365.1
10.353	55113.7	8.853	20823.9	9.683	31840.0	10.184	53010.0	8.681	22594.9
10.330	55318.9	8.577	20682.1	9.574	29407.7	9.643	30427.1	8.661	22203.5
10.229	50709.0	8.501	18113.7	9.568	29434.1	10.190	52692.8	8.667	22672.1
10.200	50517.5	8.492	18058.8	9.450	30199.6	10.024	44457.7	7.898	18765.2
10.180	50816.0	8.499	18269.6	9.566	29404.9	9.991	43808.8	7.689	16734.8
10.112	45722.6	7.719	16956.2	9.027	27884.4	9.972	43968.4	7.778	17493.6
10.103	45885.5	7.787	15367.2	9.012	27862.7	9.808	34897.2	7.688	16129.8
10.074	45283.7	7.756	17268.7	8.796	26061.9	9.813	35012.8	7.016	16186.8
10.023	41985.6	7.187	13632.1	8.892	25278.4	9.282	30843.2	7.032	16309.8
9.972	40758.1	7.203	13612.2	8.930	25325.2	9.293	30908.6	5.867	12457.8
9.812	32430.1	7.175	15473.3	8.800	23815.7	9.296	31056.1	5.835	10784.8
9.806	33109.5	10.615	77166.7	8.840	24609.7	8.592	20948.7	5.833	12556.9
9.811	33397.9	10.602	76991.8	8.867	23881.9	8.579	20811.7		
9.597	28139.9	10.596	76544.6	7.458	15254.3	8.563	20881.6		
9.524	30884.5	10.596	76544.6	7.402	15028.8	8.398	19840.7		
9.587	29191.0	10.436	64851.8	7.367	15098.4	8.421	20336.4		
9.312	28945.9	10.392	64890.2	10.615	76070.2	7.257	15064.2		
9.338	28862.6	10.336	65476.0	10.636	77280.7	7.222	15144.9		
9.346	28760.1	10.306	57889.6	10.641	77489.4	7.209	15407.7		
			58126.3	10.489	68287.0	6.903	13952.7		

Table 3 Number of test days and data points

Fluid (% mass)	Number of days	Number of data points
R123/isopentane (99.9/0.1)	7	186
R123/isopentane (99.5/0.5)	5	130
R123/isopentane (99/1)	2	64
R123/pentane (99.5/0.5)	3	113
R123/pentane (99/1)	4	113
R123/hexane (99.5/0.5)	5	158
R123/hexane (99/1)	6	175
R123/heptane (99.5/0.5)	5	111
R123/cyclohexane (99.5/0.5)	6	177
R123/cyclohexane (99/1)	7	182
R123	8	276

Table 4 Constants for cubic boiling curve fits for GEWA-T™

$$\Delta T_s = A_0 + A_1 q'' + A_2 q''^2 + A_3 q''^3$$

ΔT_s in Kelvins and q'' in W/m^2

Fluid		A_0	A_1	A_2	A_3
R123/isopentane (99.9/0.1)	$\Delta T_s \geq 8.5K$	5.162564	2.213069×10^{-4}	-3.305539×10^{-9}	1.794215×10^{-14}
	$\Delta T_s \leq 9.5K$	3.242045	2.982389×10^{-4}	$-9.070653 \times 10^{-10}$	-7.87954×10^{-14}
R123/isopentane (99.5/0.5)	$\Delta T_s \geq 8K$	6.596237	1.387433×10^{-4}	-1.89345×10^{-9}	9.752913×10^{-15}
	$\Delta T_s \leq 9.5K$	-1.953420	1.143663×10^{-3}	-4.152663×10^{-8}	5.346848×10^{-13}
R123/isopentane (99/1)	$\Delta T_s \geq 0K$	6.239937	1.715029×10^{-4}	-2.614962×10^{-9}	1.441917×10^{-14}
	$\Delta T_s \leq 10K$	-5.436468	1.228280×10^{-3}	-3.369096×10^{-8}	3.120554×10^{-13}
R123/pentane (99.5/0.5)	$\Delta T_s \geq 9.7K$	8.725847	5.269372×10^{-5}	$-5.821089 \times 10^{-10}$	2.857575×10^{-15}
	$\Delta T_s \leq 9.7K$	9.454738×10^{-1}	4.434199×10^{-4}	-1.626985×10^{-9}	$-1.148459 \times 10^{-13}$
R123/pentane (99/1)	$\Delta T_s \geq 9K$	6.665111	1.609068×10^{-4}	-2.494825×10^{-9}	1.396698×10^{-14}
	$\Delta T_s \leq 9K$	5.494870	-5.514591×10^{-4}	6.175966×10^{-8}	$-1.360361 \times 10^{-12}$
R123/hexane (99.5/0.5)	$\Delta T_s \geq 9K$	7.052807	1.128998×10^{-4}	-1.337031×10^{-9}	6.112061×10^{-15}
	$\Delta T_s \leq 9K$	2.307429	7.110618×10^{-5}	2.923709×10^{-8}	$-8.785910 \times 10^{-13}$
R123/hexane (99/1)	$\Delta T_s \geq 9.5K$	8.415715	4.340422×10^{-5}	$-1.416185 \times 10^{-10}$	$-6.081541 \times 10^{-16}$
	$\Delta T_s \leq 9.5K$	-8.193729	1.975566×10^{-3}	-7.828415×10^{-8}	1.061641×10^{-12}
R123/heptane (99.5/0.5)	$\Delta T_s \geq 10K$	7.642573	1.367339×10^{-4}	-1.968117×10^{-9}	1.071097×10^{-14}
	$\Delta T_s \leq 10.7K$	-4.695406×10^{-1}	8.135101×10^{-4}	-2.198312×10^{-8}	2.182051×10^{-13}
R123/cyclohexane (99.5/0.5)	$\Delta T_s \geq 9K$	5.140536	2.582199×10^{-4}	-4.229872×10^{-9}	2.413322×10^{-14}
	$\Delta T_s \leq 9K$	-3.819449	1.137466×10^{-3}	-2.584559×10^{-8}	2.736247×10^{-15}
R123/cyclohexane (99/1)	$\Delta T_s \geq 0K$	3.727304	3.204812×10^{-4}	-5.075217×10^{-9}	2.809359×10^{-14}
R123	$\Delta T_s \geq 9K$	6.21063	1.71370×10^{-4}	-2.475810×10^{-9}	1.287840×10^{-14}
	$\Delta T_s \leq 9.7K$	-3.71984	1.21909×10^{-3}	-3.952890×10^{-8}	4.497650×10^{-13}

Table 5 Residual standard deviation of q'' data from the mean ΔT_s

Fluid	Low q'' U (K)	High q'' U (K)
R123/isopentane (99.9/0.1)	(<9.5K) 0.18	(>8.5K) 0.13
R123/isopentane (99.5/0.5)	(<9.5K) 0.12	(>8K) 0.10
R123/isopentane (99/1)	(<10K) 0.18	(>0K) 0.12
R123/pentane (99.5/0.5)	(<9.7K) 0.26	(>9.7K) 0.04
R123/pentane (99/1)	(<9K) 0.21	(>9K) 0.08
R123/hexane (99.5/0.5)	(<9K) 0.13	(>9K) 0.11
R123/hexane (99/1)	(<9.5K) 0.15	(>9.5K) 0.06
R123/heptane (99.5/0.5)	(<10.7K) 0.16	(>10K) 0.08
R123/cyclohexane (99.5/0.5)	(<9K) 0.19	(>9K) 0.10
R123/cyclohexane (99/1)	(<0K) 0.14	(>0K) 0.14
R123	(<9.7K) 0.25	(>9K) 0.11

Table 6 Average magnitude of 95% multi-use confidence interval for mean $T_w - T_s$ (K)

Fluid	Low q'' U (K)	High q'' U (K)
R123/isopentane (99.9/0.1)	0.16	0.07
R123/isopentane (99.5/0.5)	0.13	0.06
R123/isopentane (99/1)	0.21	0.10
R123/pentane (99.5/0.5)	0.24	0.04
R123/pentane (99/1)	0.22	0.07
R123/hexane (99.5/0.5)	0.15	0.04
R123/hexane (99/1)	0.13	0.04
R123/heptane (99.5/0.5)	0.15	0.06
R123/cyclohexane (99.5/0.5)	0.26	0.06
R123/cyclohexane (99/1)	0.07	0.07
R123	0.15	0.05

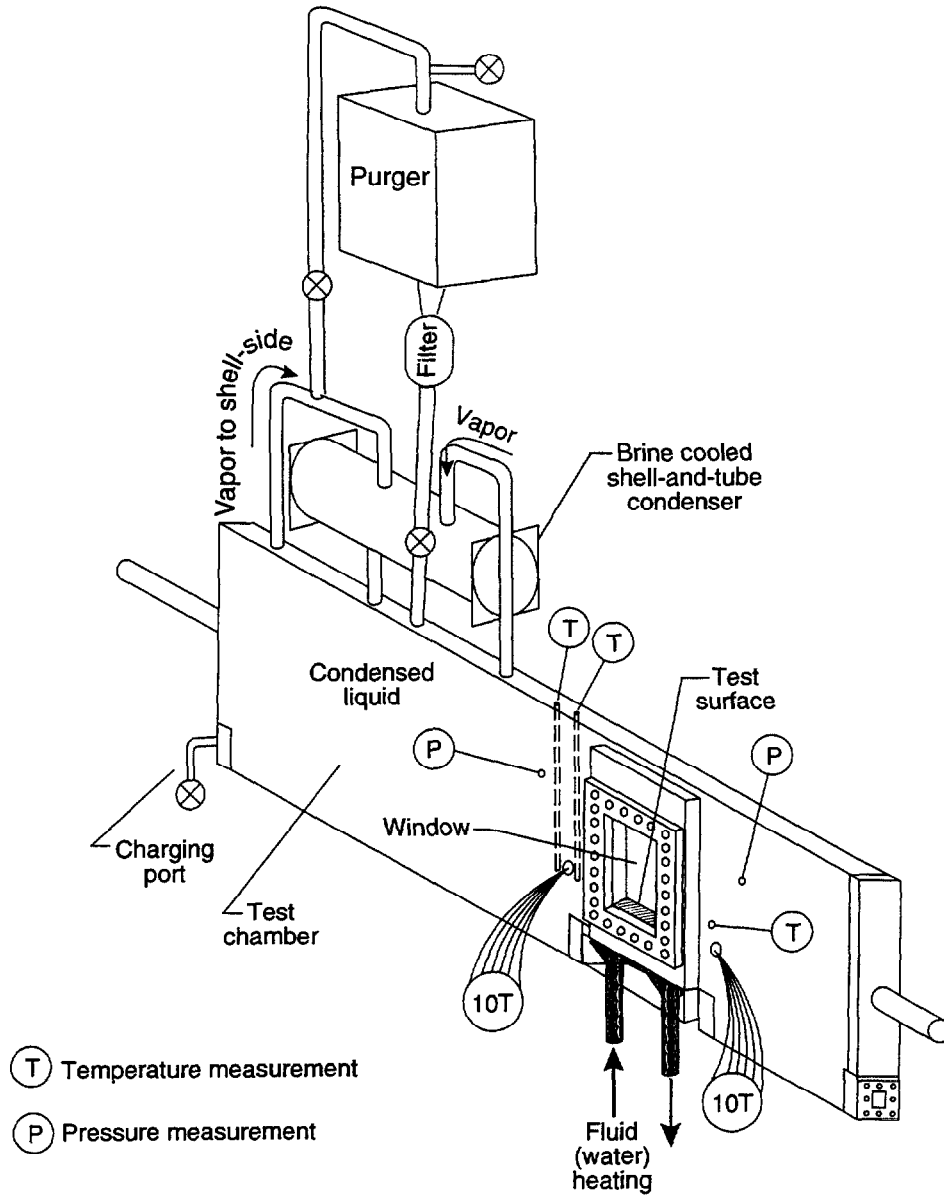


Fig. 1 Schematic of test apparatus

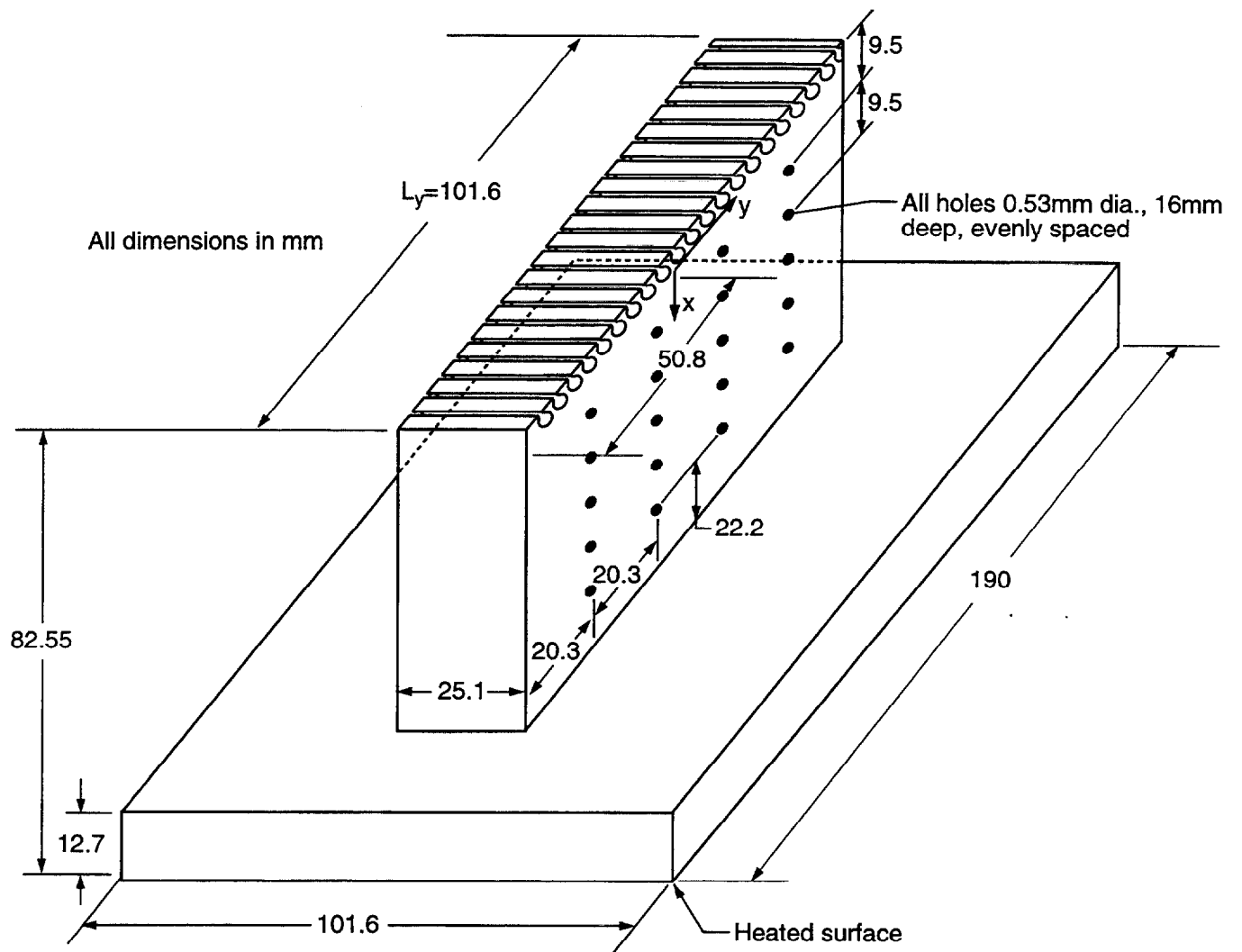


Fig. 2 OFHC copper GEWA-TTM test plate and thermocouple coordinate system

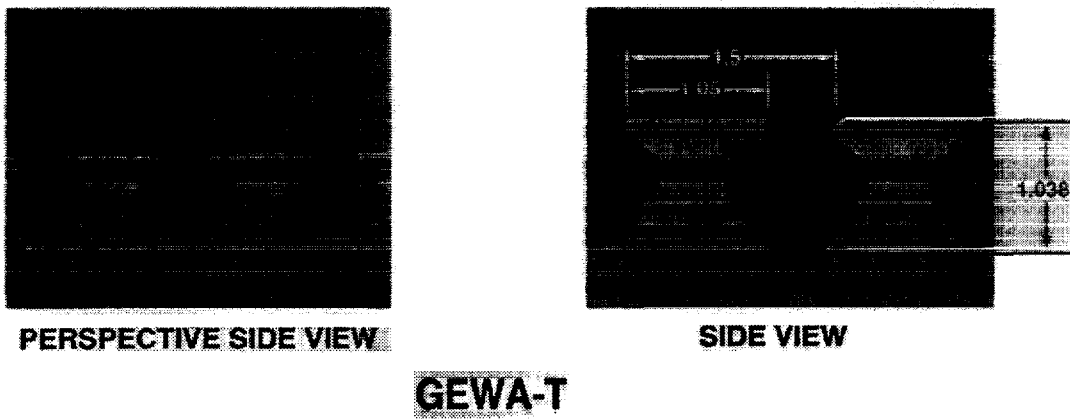


Fig. 3 Photograph of GEWA-TTM geometry

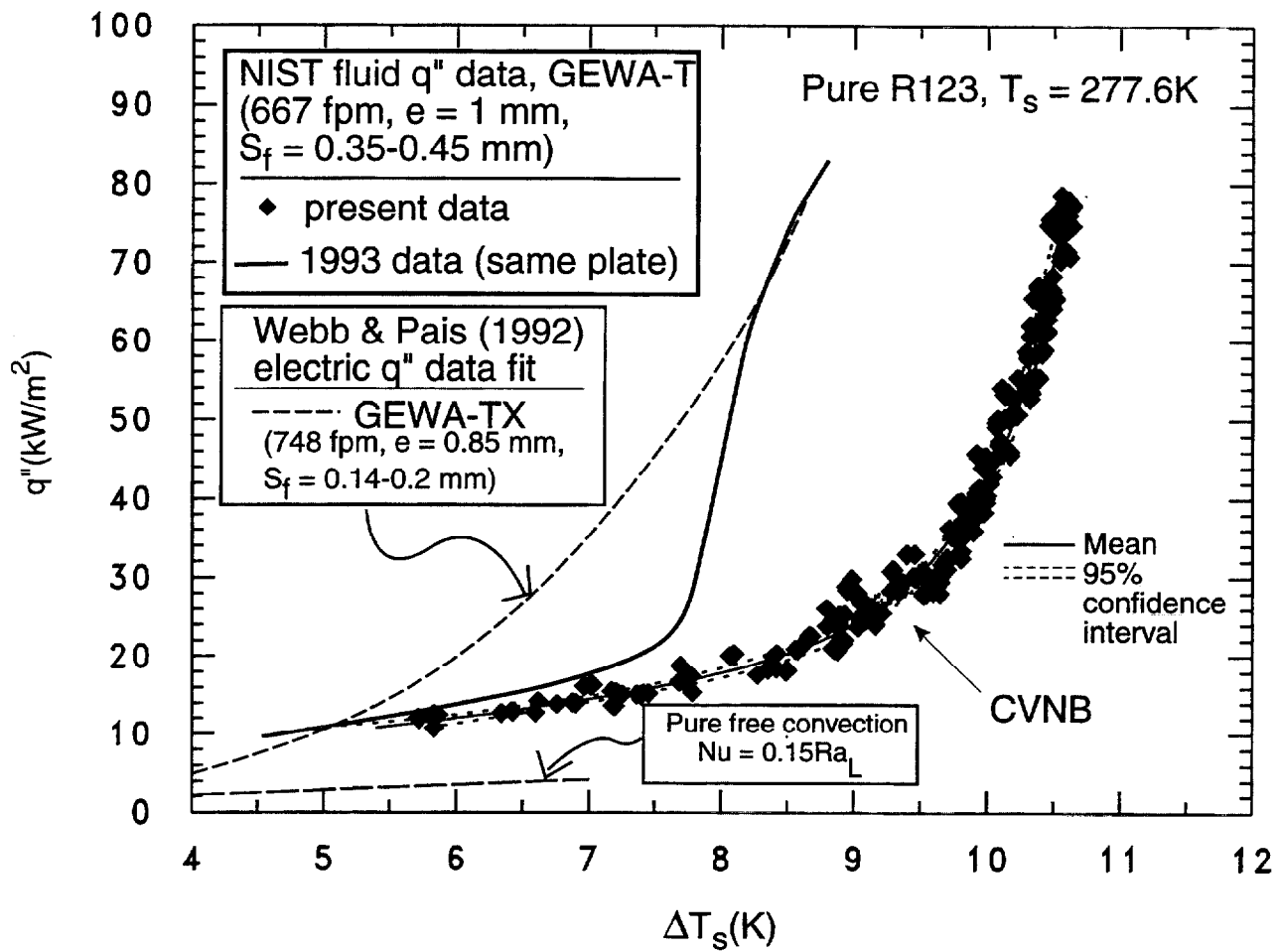


Fig. 4 R123 pool boiling curve for GEWA-T surface at 277.6 K

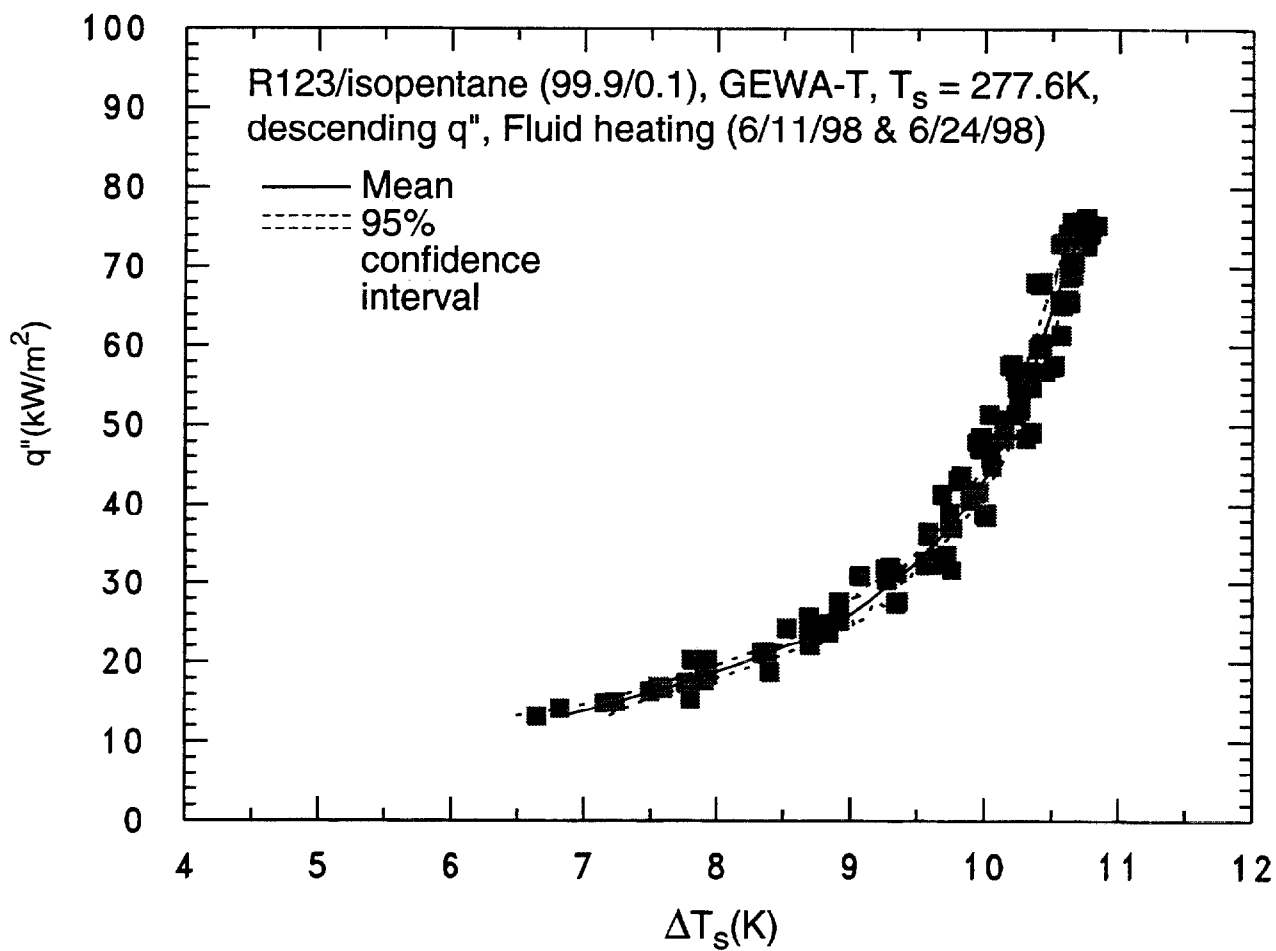


Fig. 5 R123/isopentane (99.9/0.1) pool boiling curve for GEWA-T surface at 277.6 K

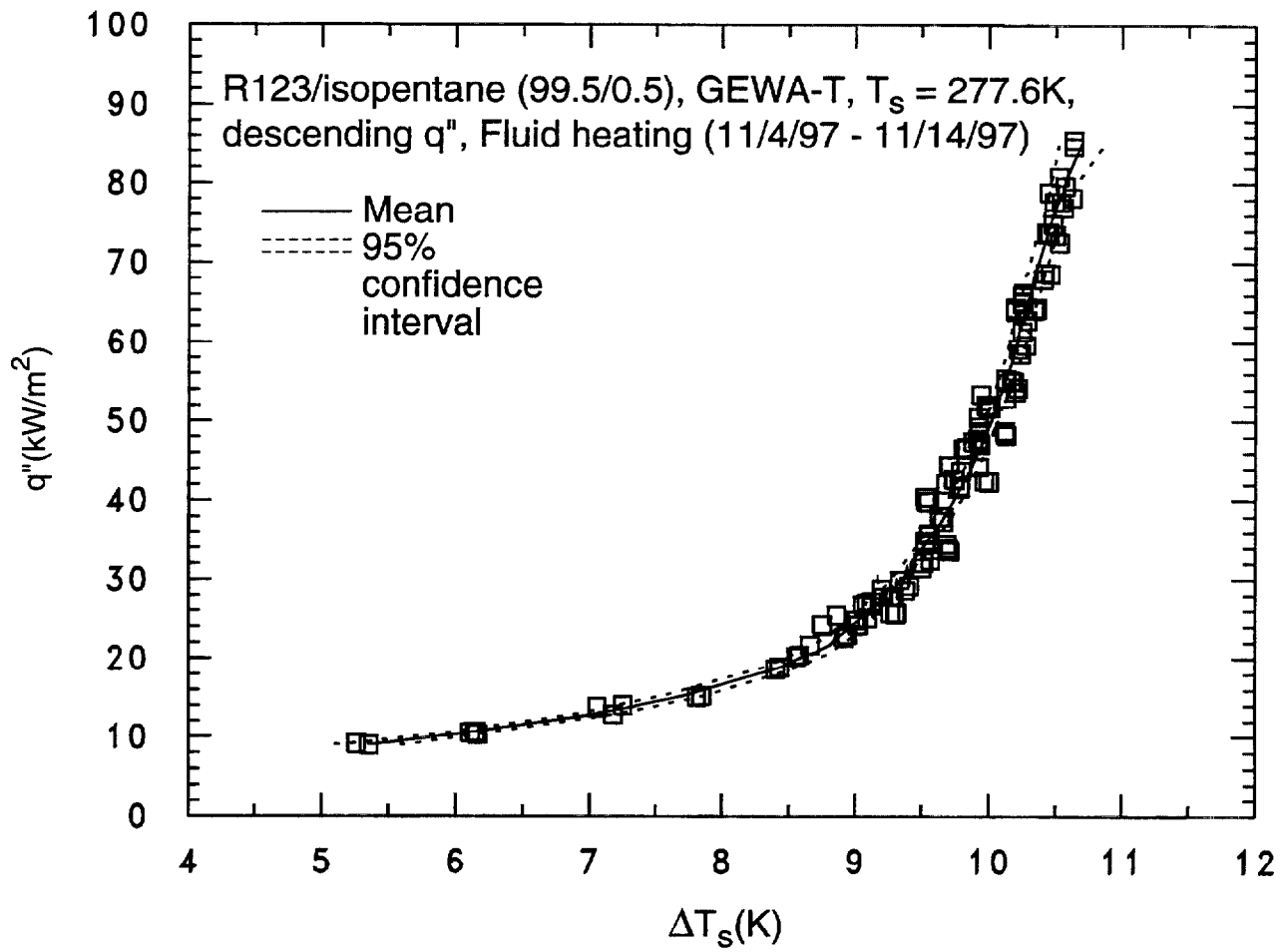


Fig. 6 R123/isopentane (99.5/0.5) pool boiling curve for GEWA-T surface at 277.6 K

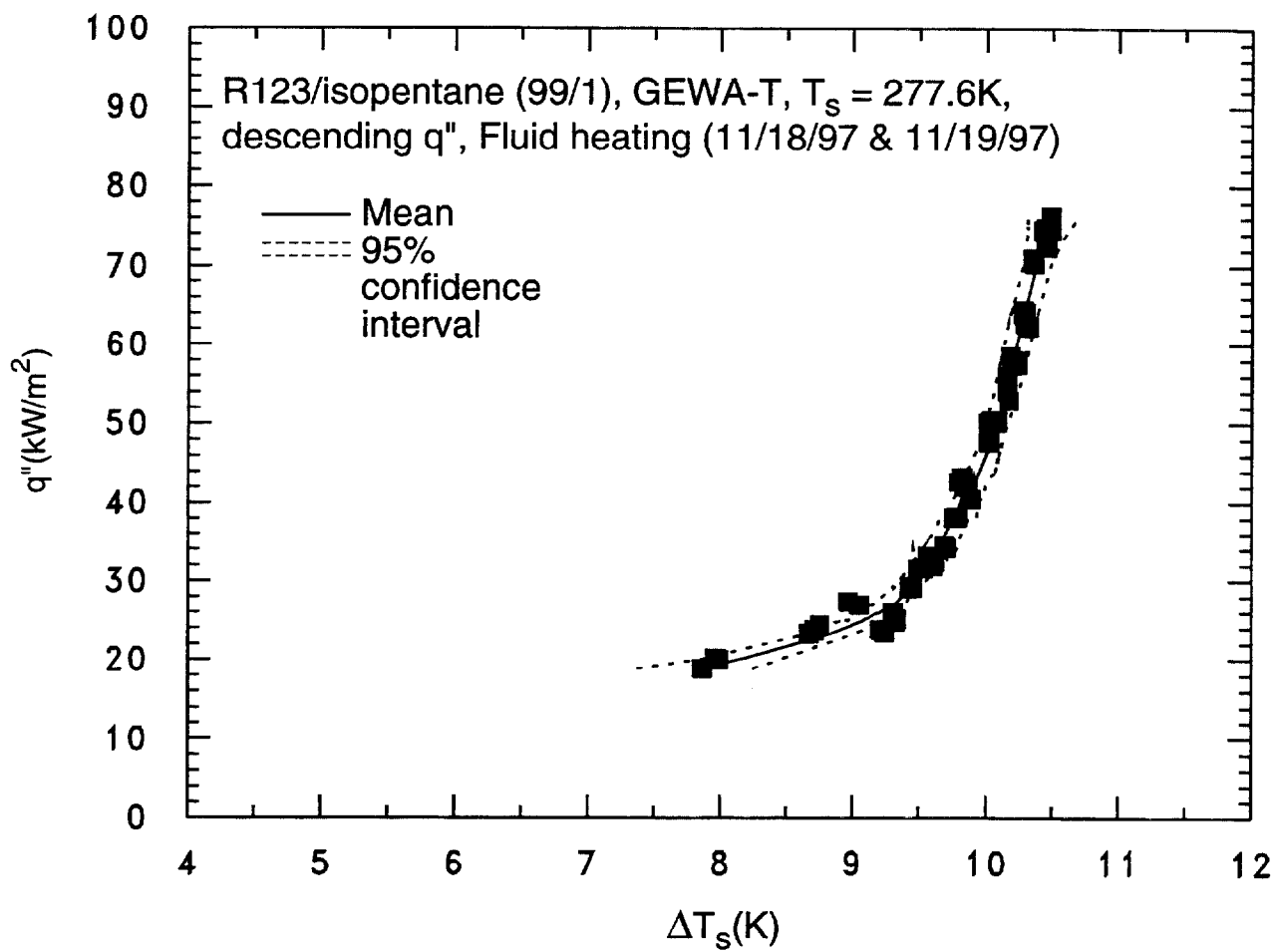


Fig. 7 R123/isopentane (99/1) pool boiling curve for GEWA-T surface at 277.6 K

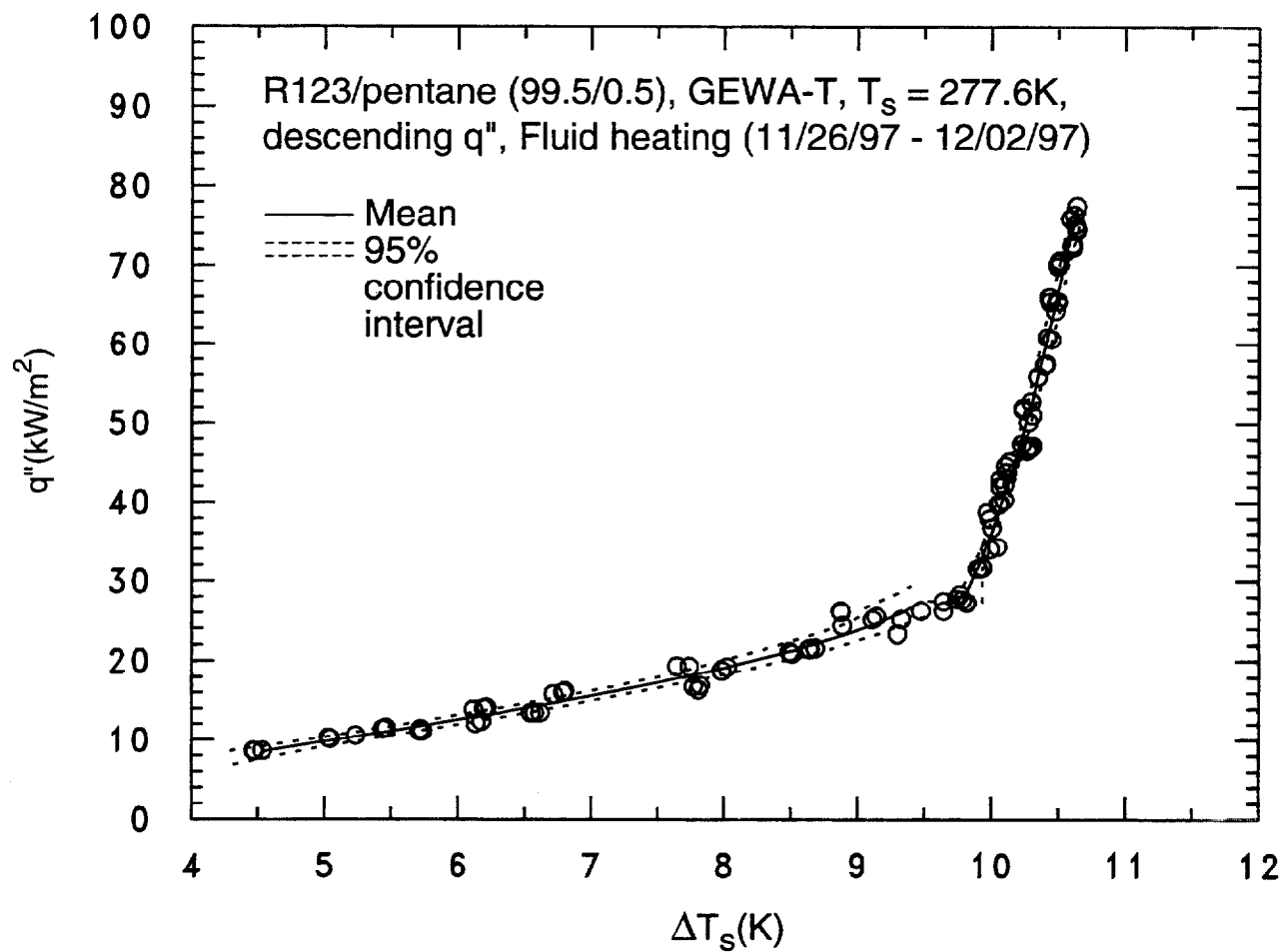


Fig. 8 R123/pentane (99.5/0.5) pool boiling curve for GEWA-T surface at 277.6 K

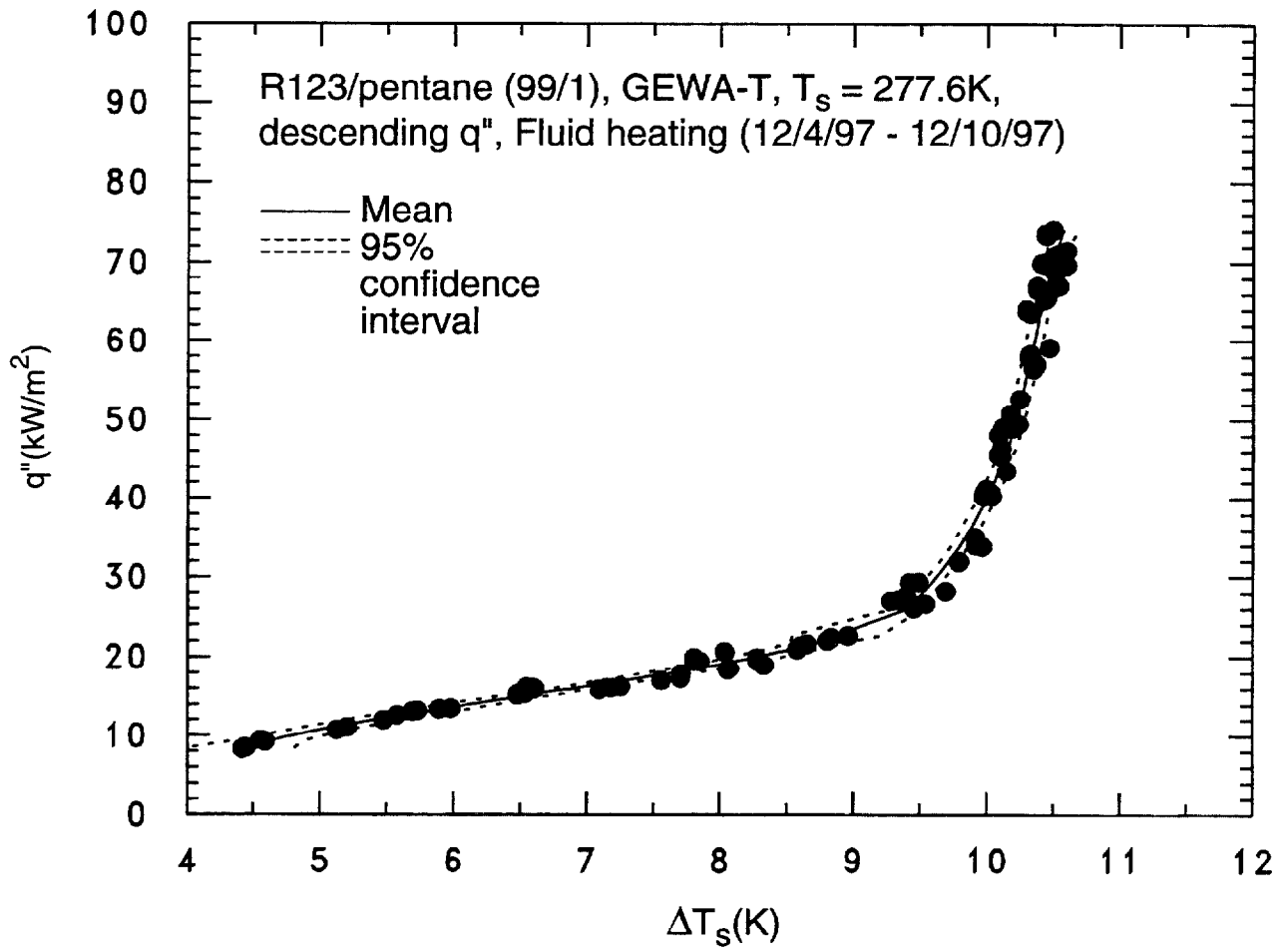


Fig. 9 R123/pentane (99/1) pool boiling curve for GEWA-T surface at 277.6 K

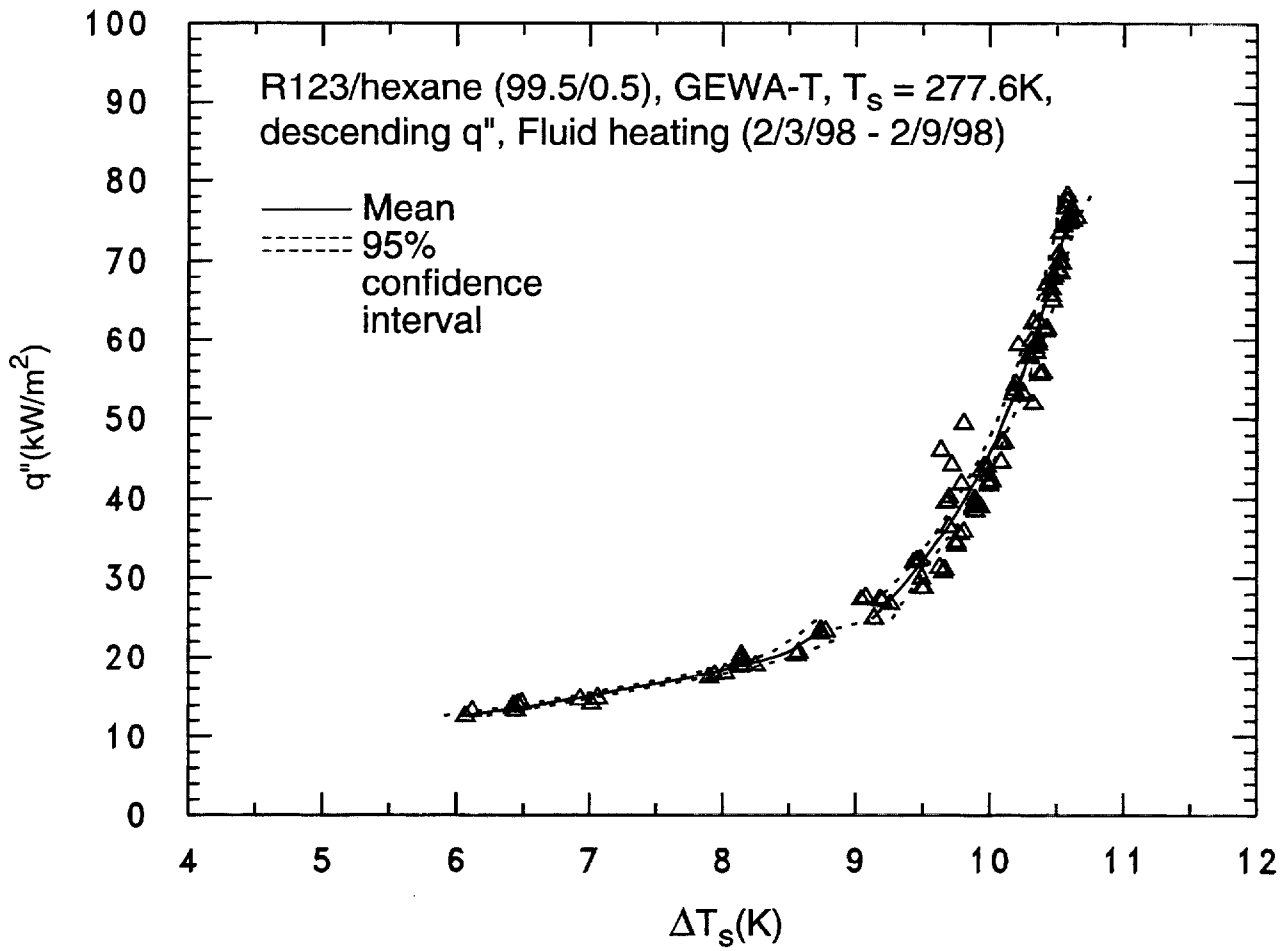


Fig. 10 R123/hexane (99.5/0.5) pool boiling curve for GEWA-T surface at 277.6 K

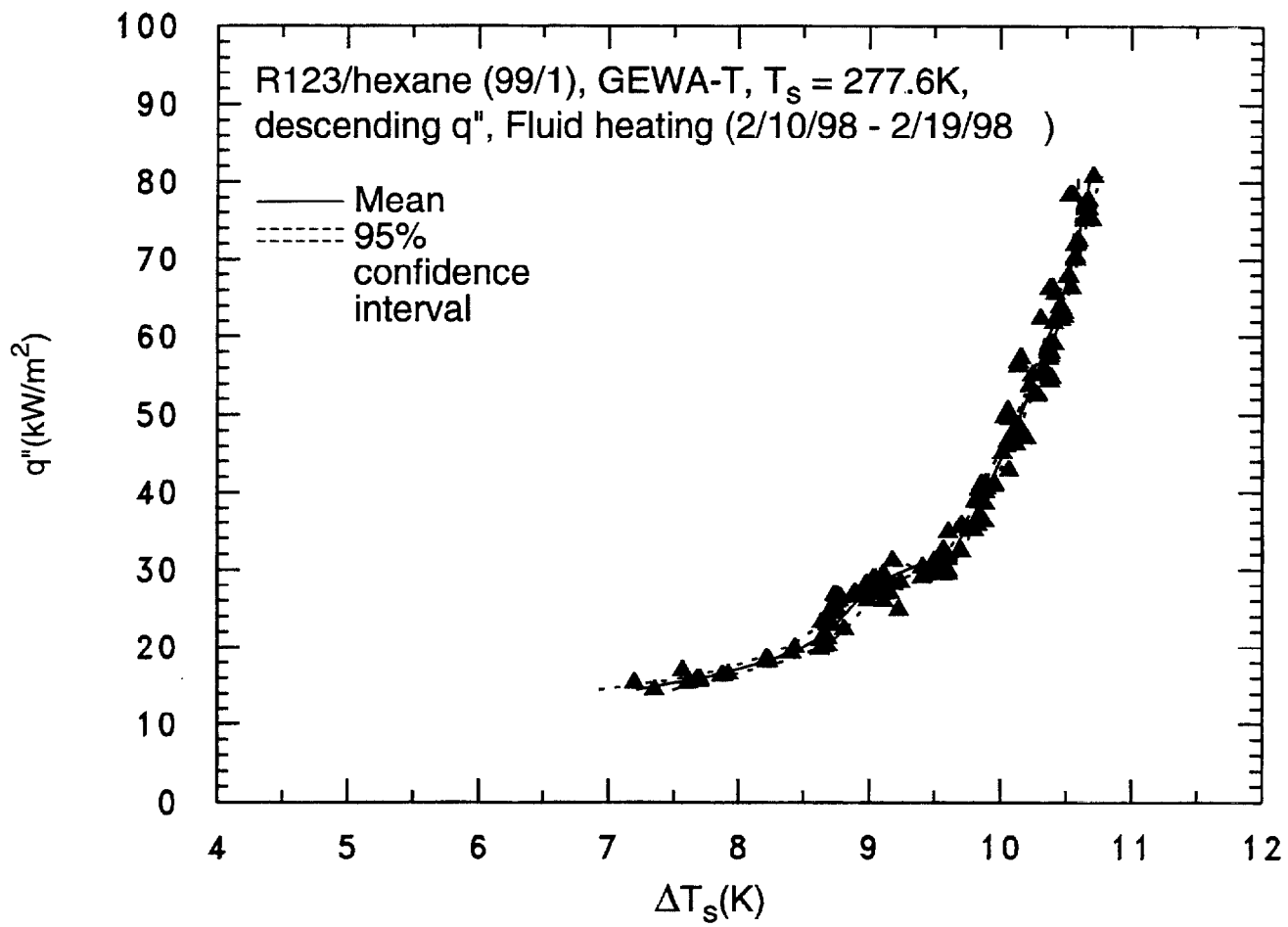


Fig. 11 R123/hexane (99/1) pool boiling curve for GEWA-T surface at 277.6 K

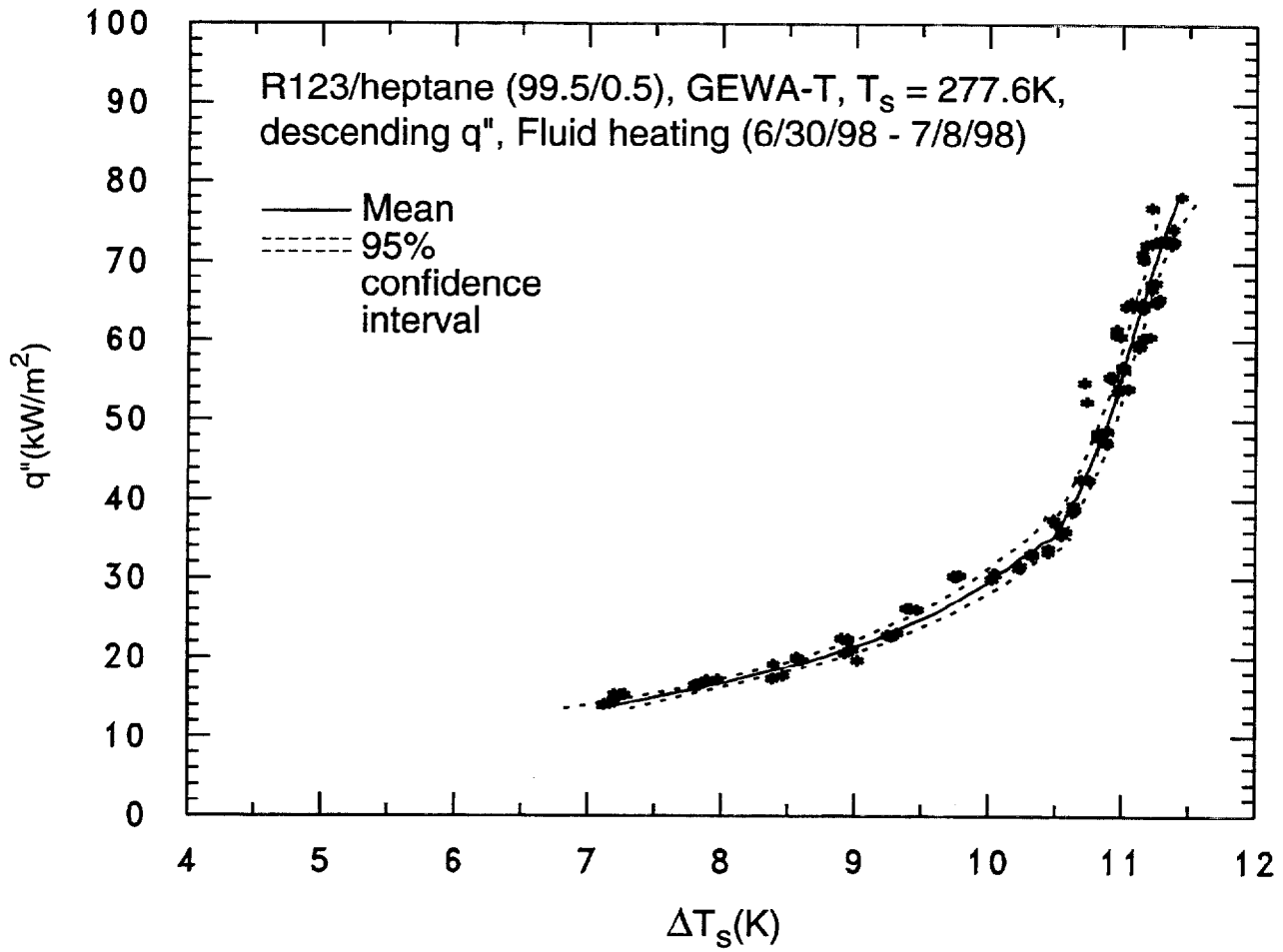


Fig. 12 R123/heptane (99.5/0.5) pool boiling curve for GEWA-T surface at 277.6 K

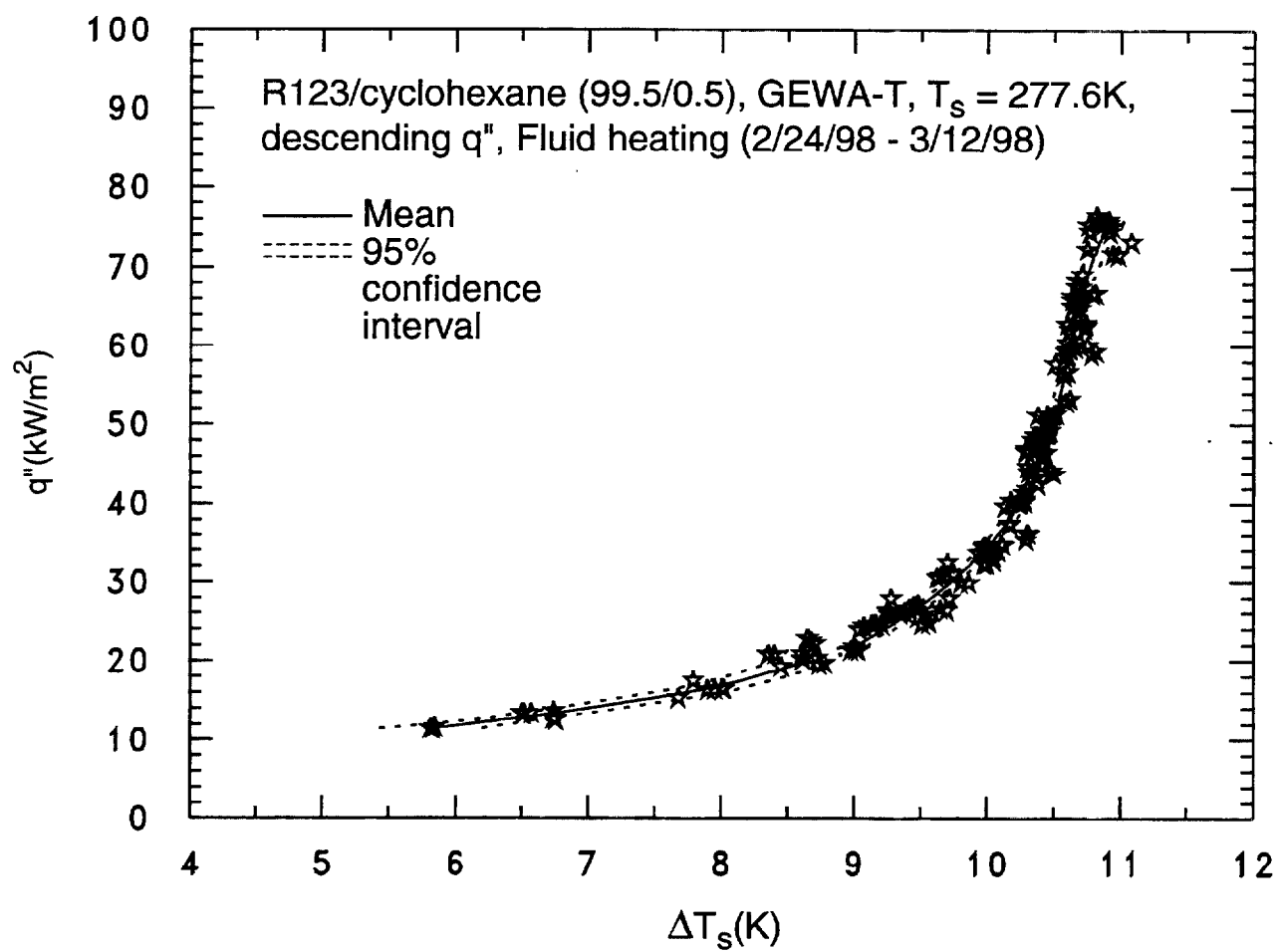


Fig. 13 R123/cyclohexane (99.5/0.5) pool boiling curve for GEWA-T surface at 277.6 K

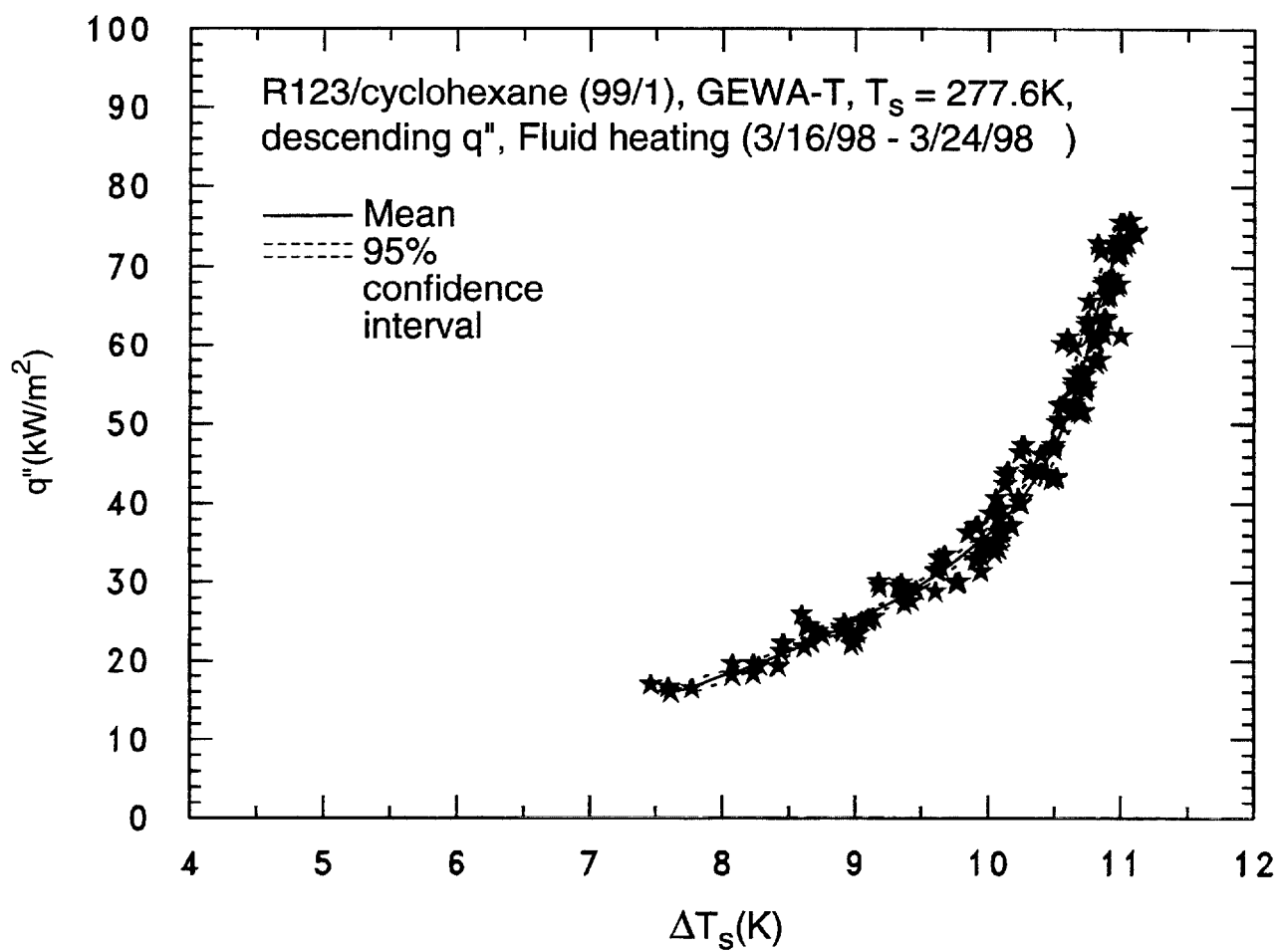


Fig. 14 R123/cyclohexane (99/1) pool boiling curve for GEWA-T surface at 277.6 K

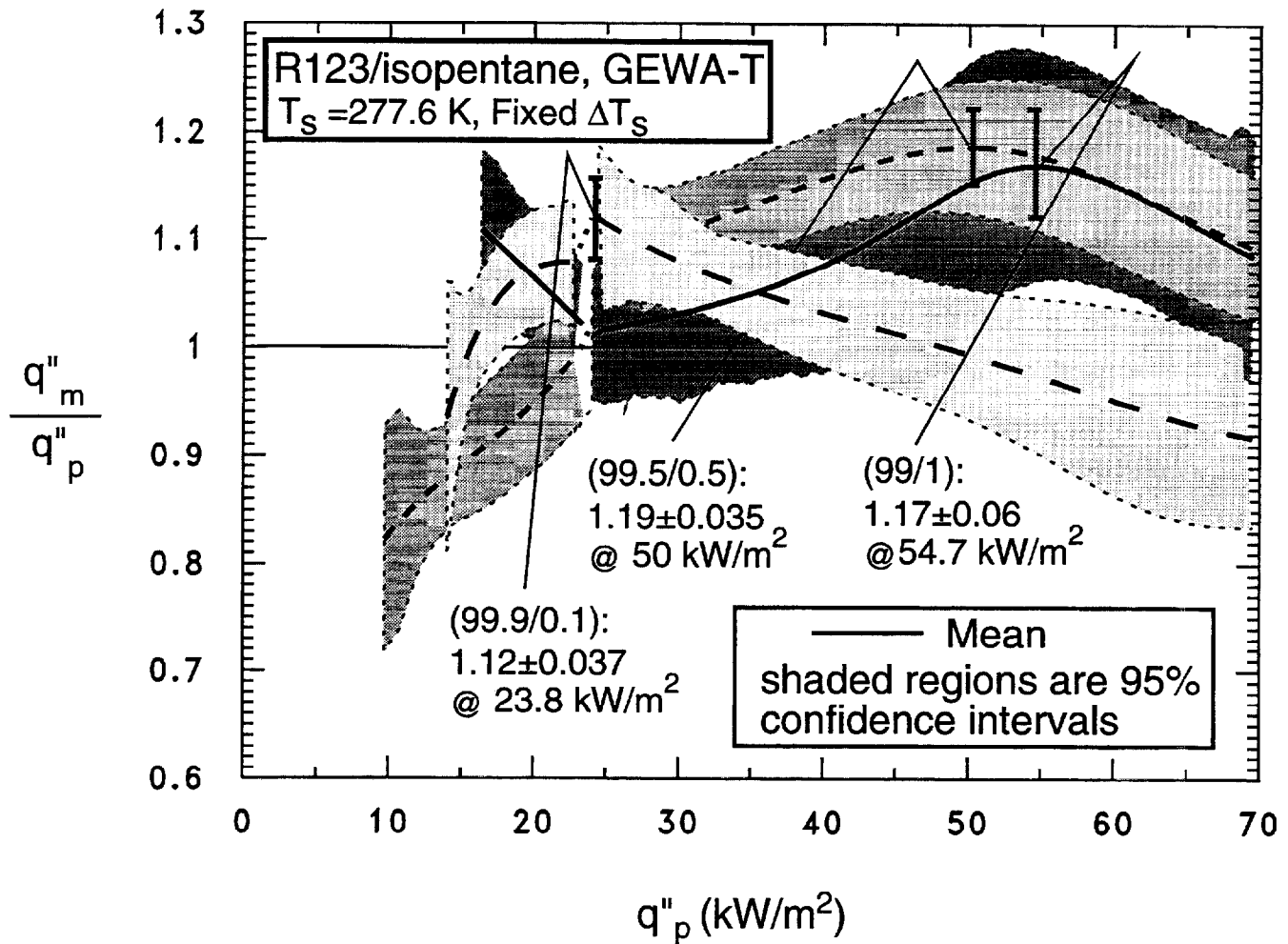


Fig. 15 Enhancement ratio for three dilute R123/isopentane mixtures

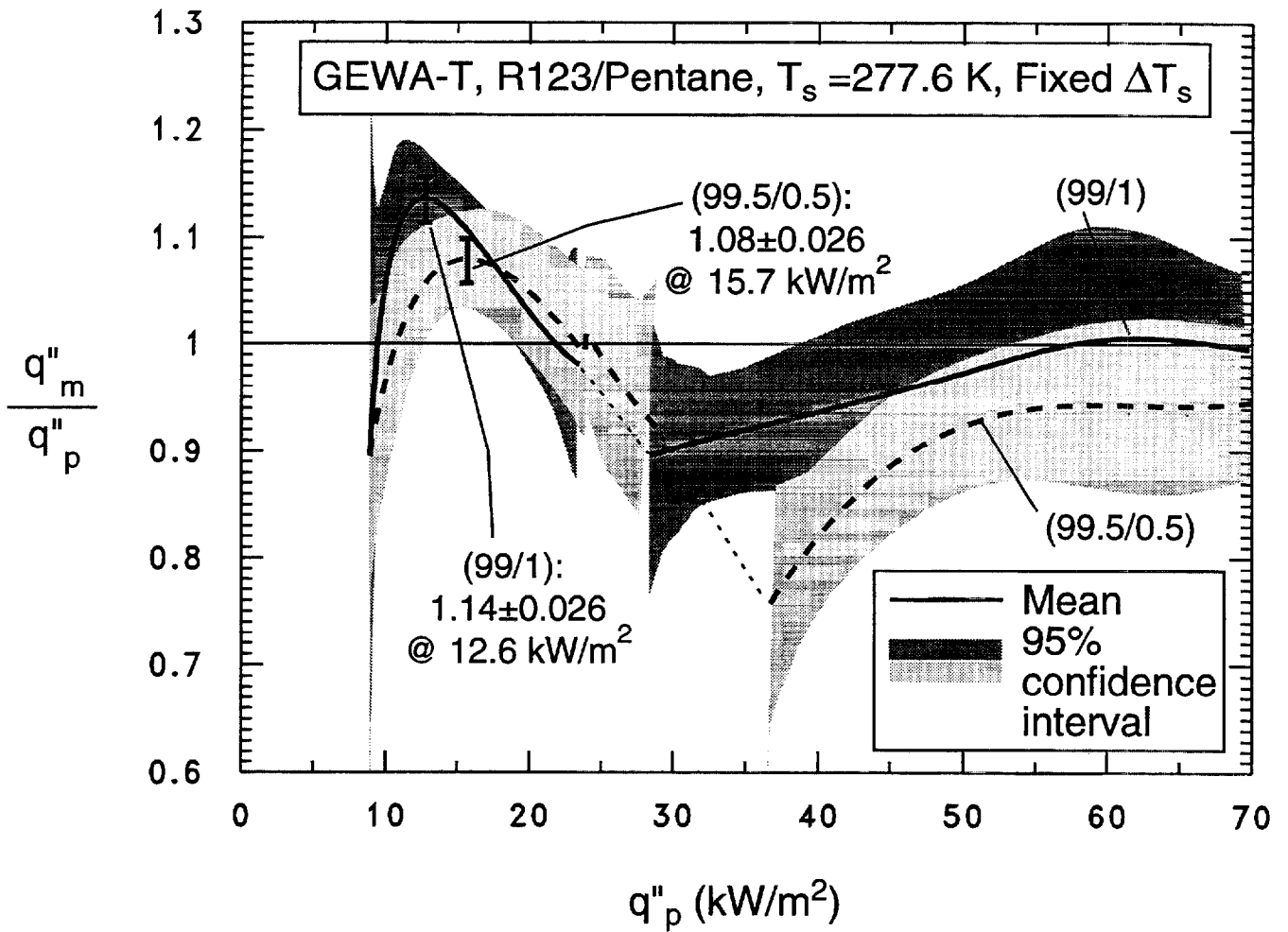


Fig. 16 Enhancement ratio for two dilute R123/pentane mixtures

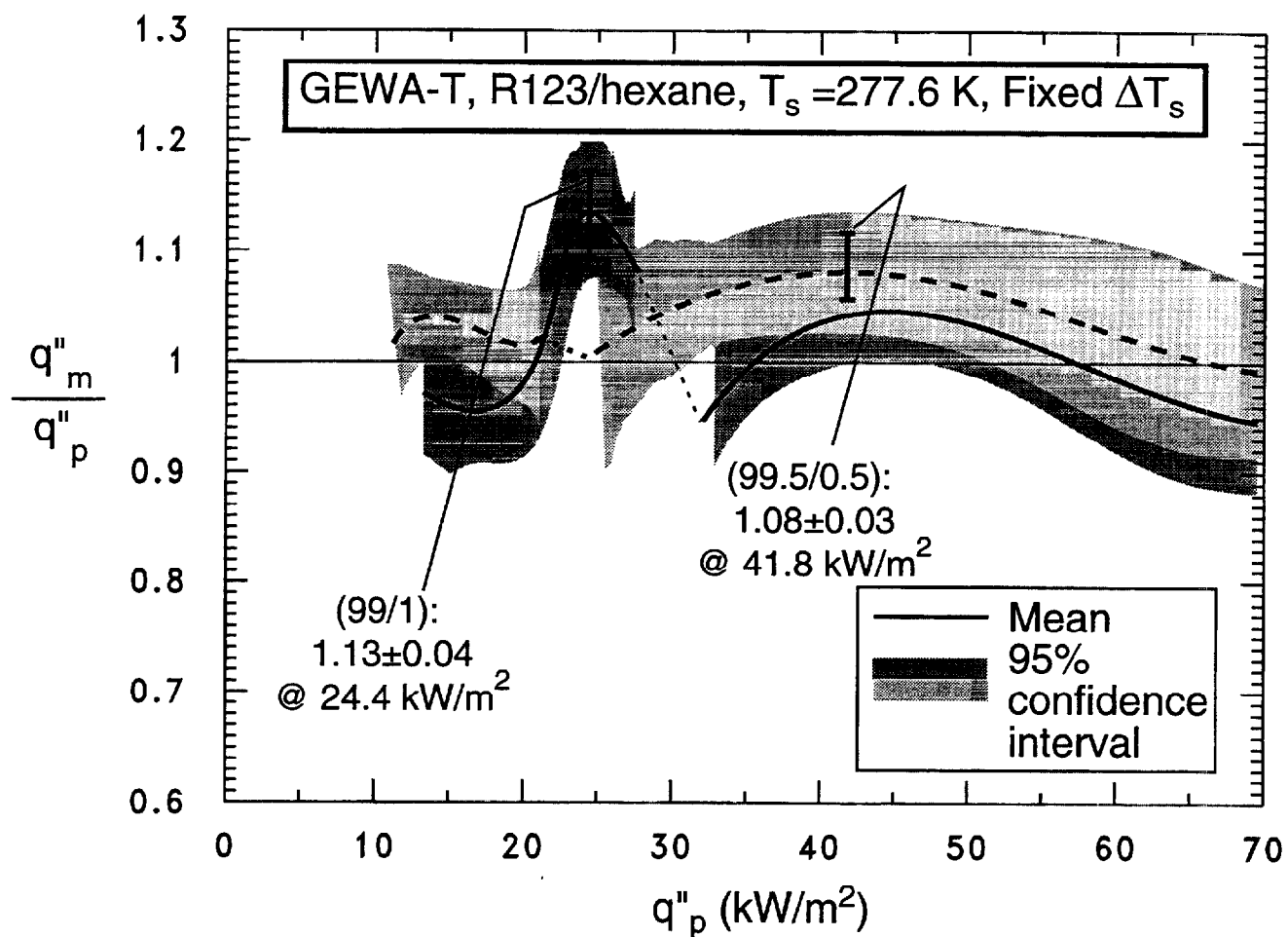


Fig. 17 Enhancement ratio for two dilute R123/hexane mixtures

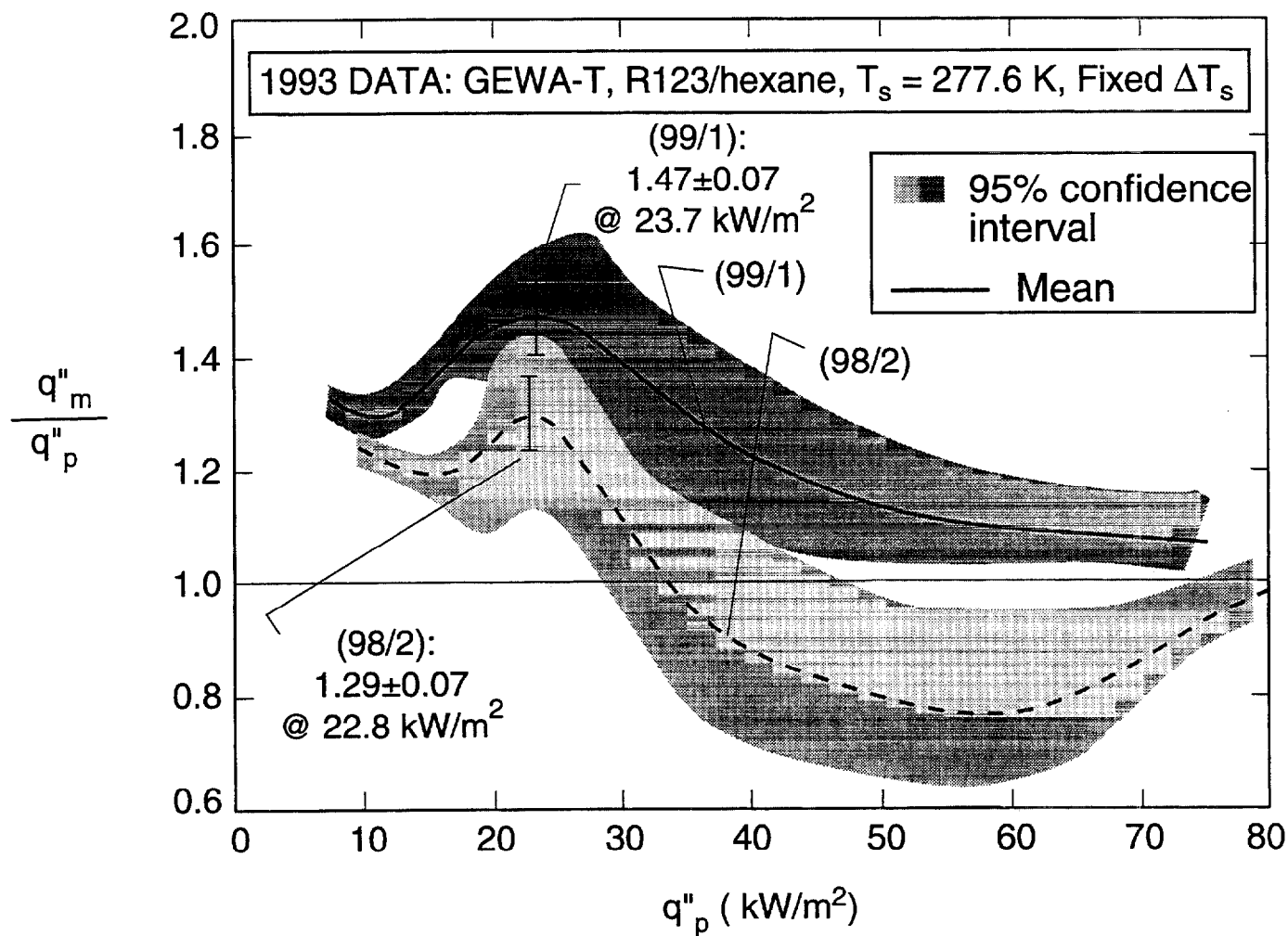


Fig .18 Effect of hexane on R123 pool boiling heat flux as measured in 1993

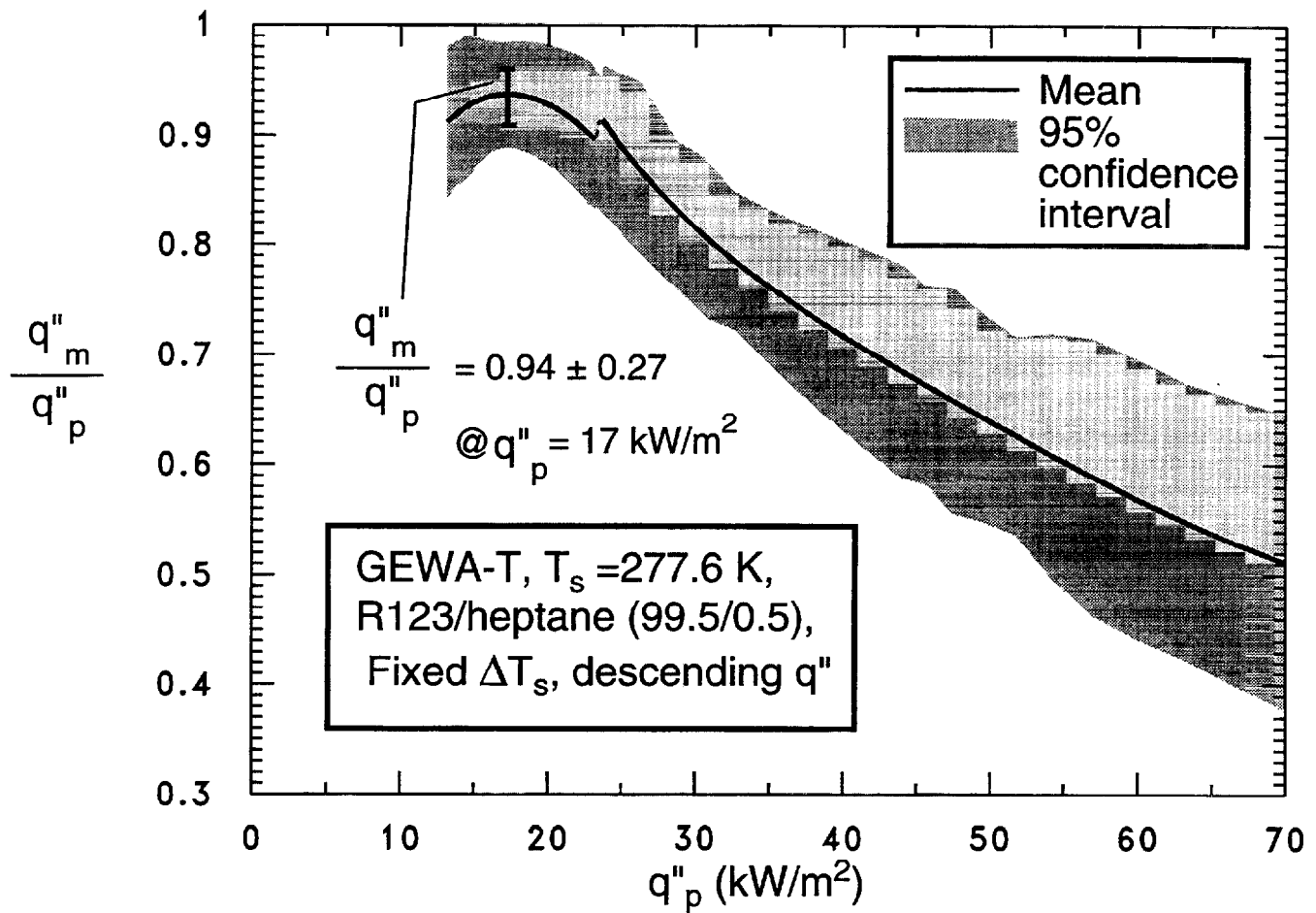


Fig. 19 Enhancement ratio for R123/heptane (99.5/0.5)

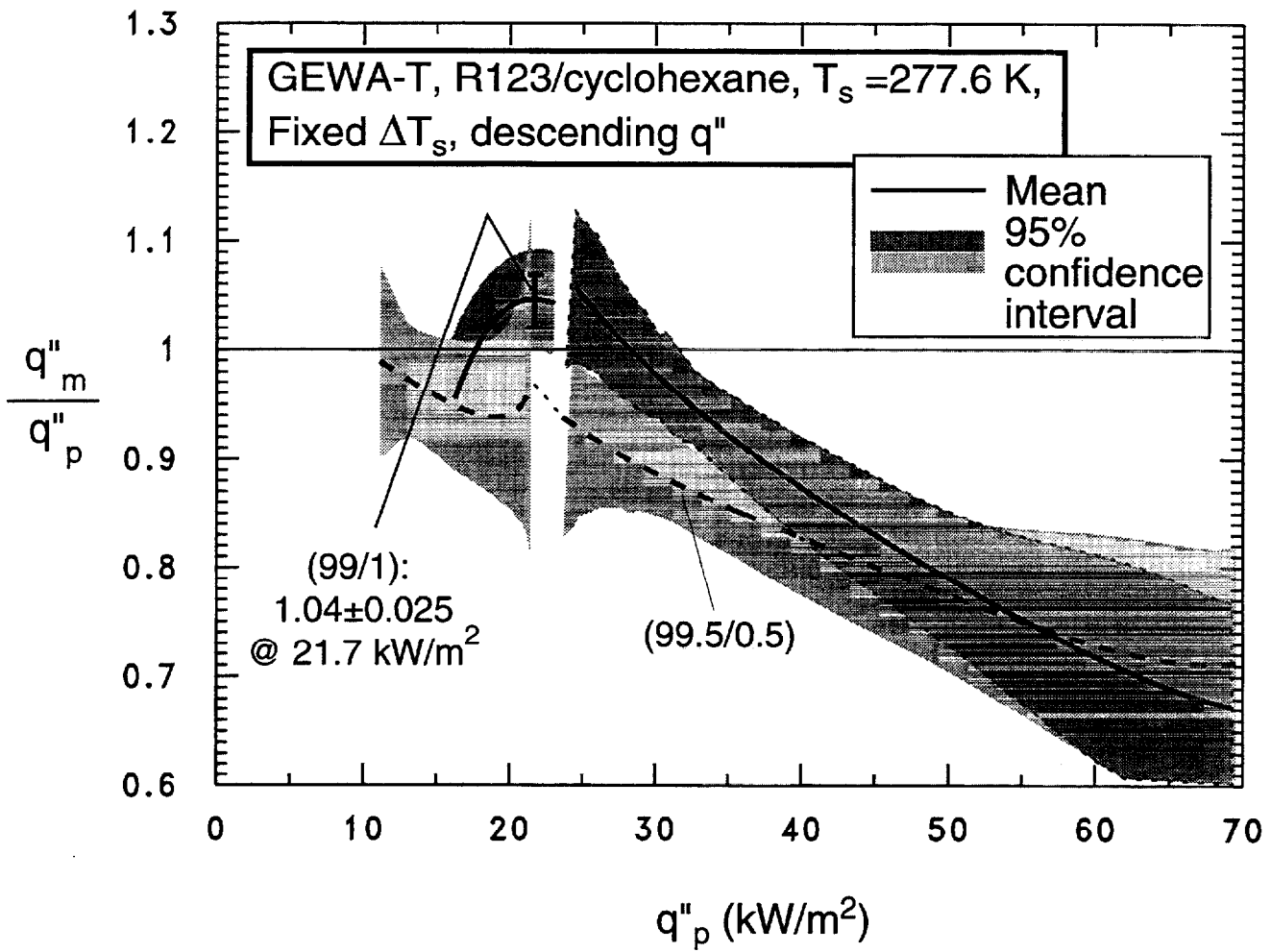


Fig. 20 Enhancement ratio for two dilute R123/cyclohexane mixtures

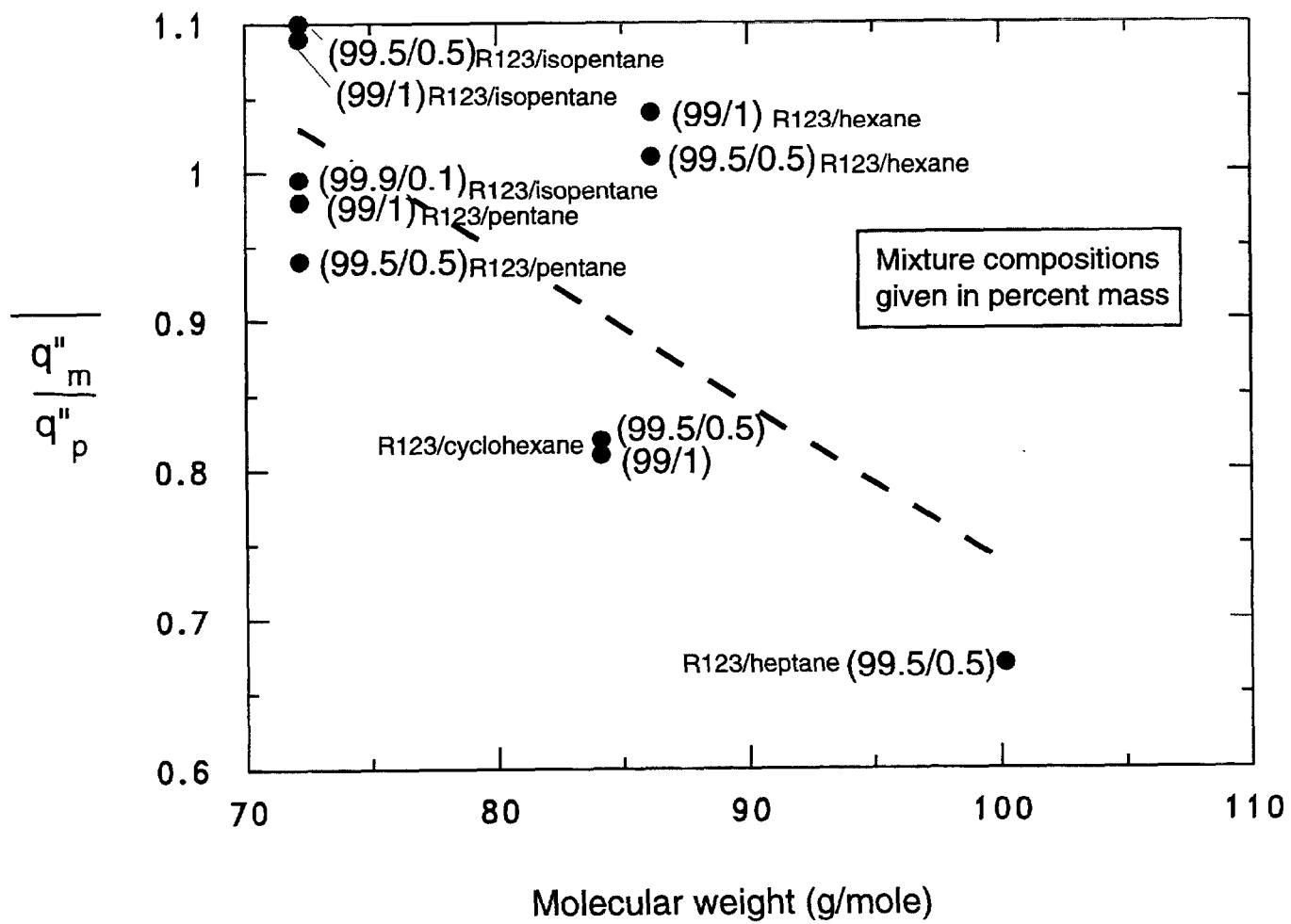


Fig. 21 Influence of molecular weight on the average enhancement ratio for dilute solutions of R123 and hydrocarbons

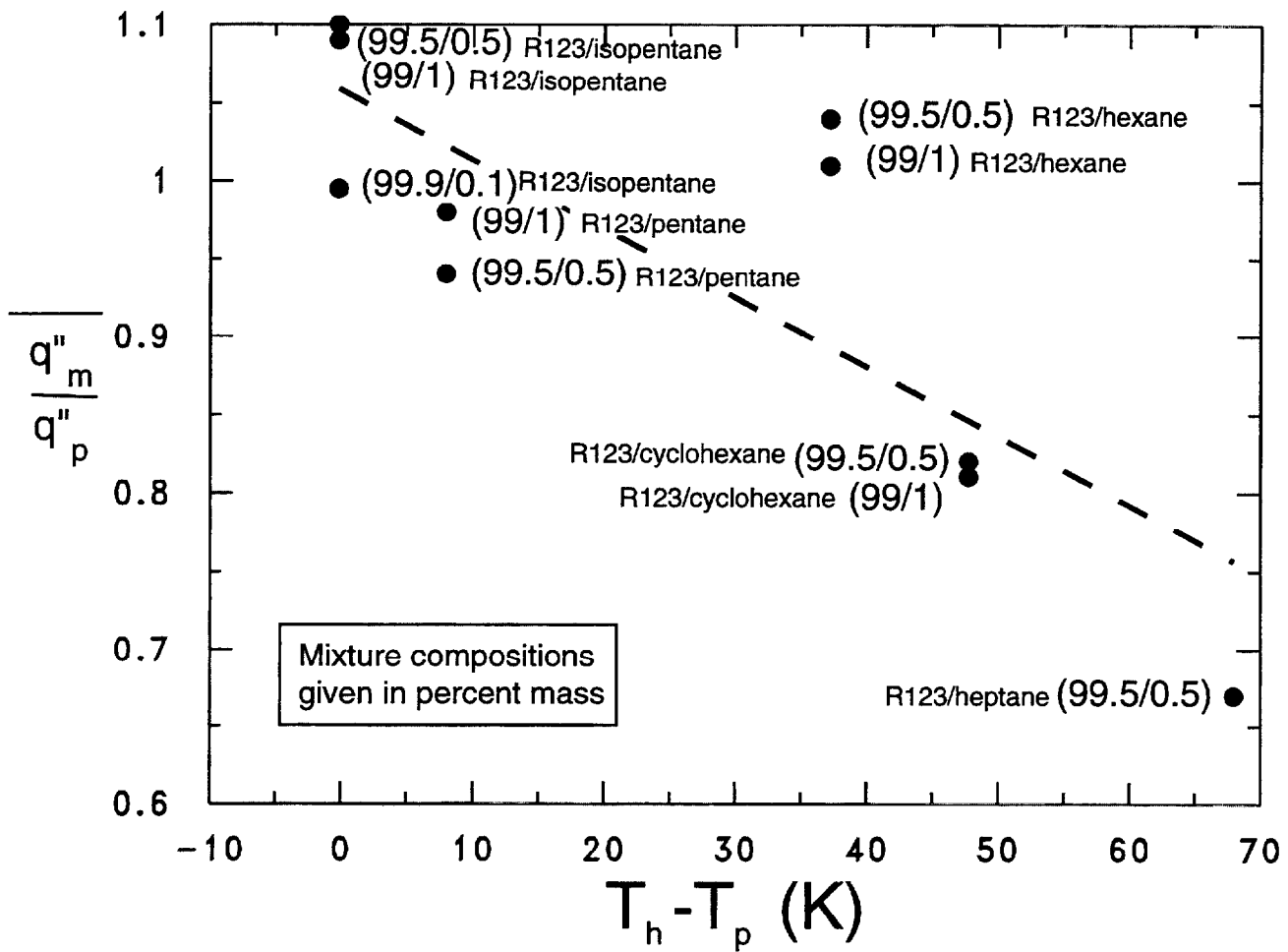


Fig. 22 Influence of boiling range on the average enhancement ratio for dilute solutions of R123 and hydrocarbons.

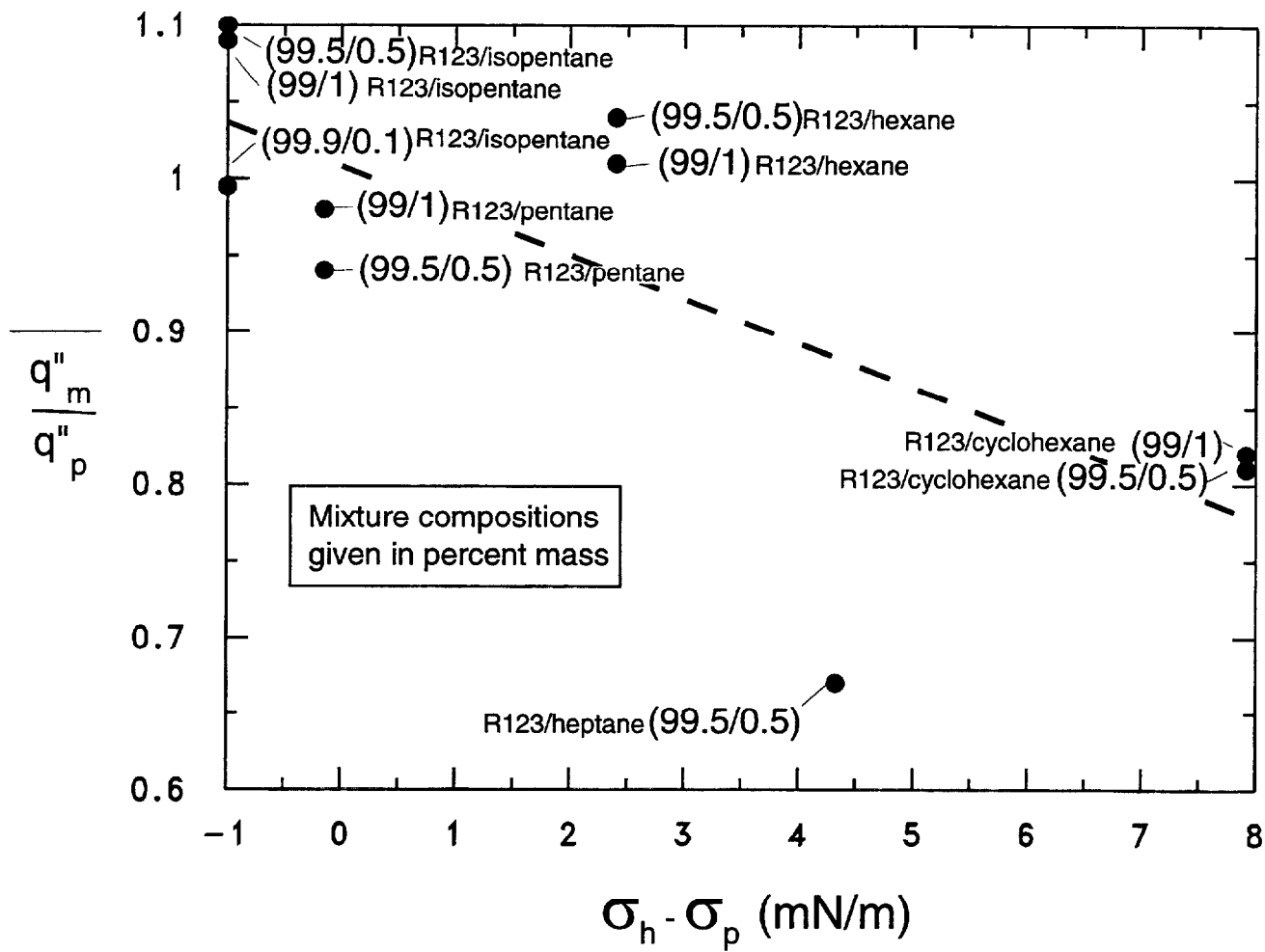


Fig. 23 Influence of surface tension on the average enhancement ratio for dilute solutions of R123 and hydrocarbons

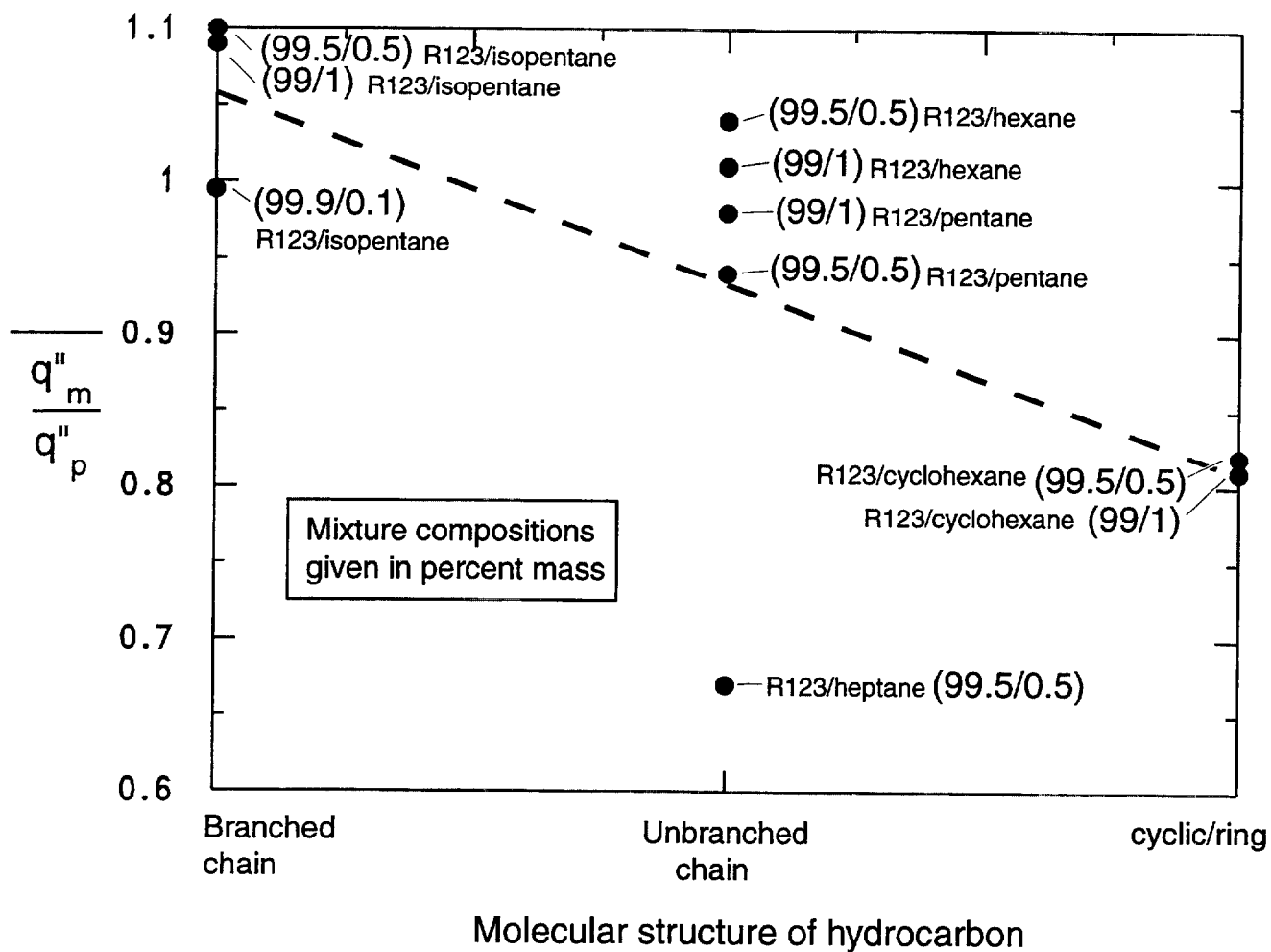


Fig. 24 Influence of molecular structure of hydrocarbon on the average enhancement ratio for dilute solutions of R123 and hydrocarbons

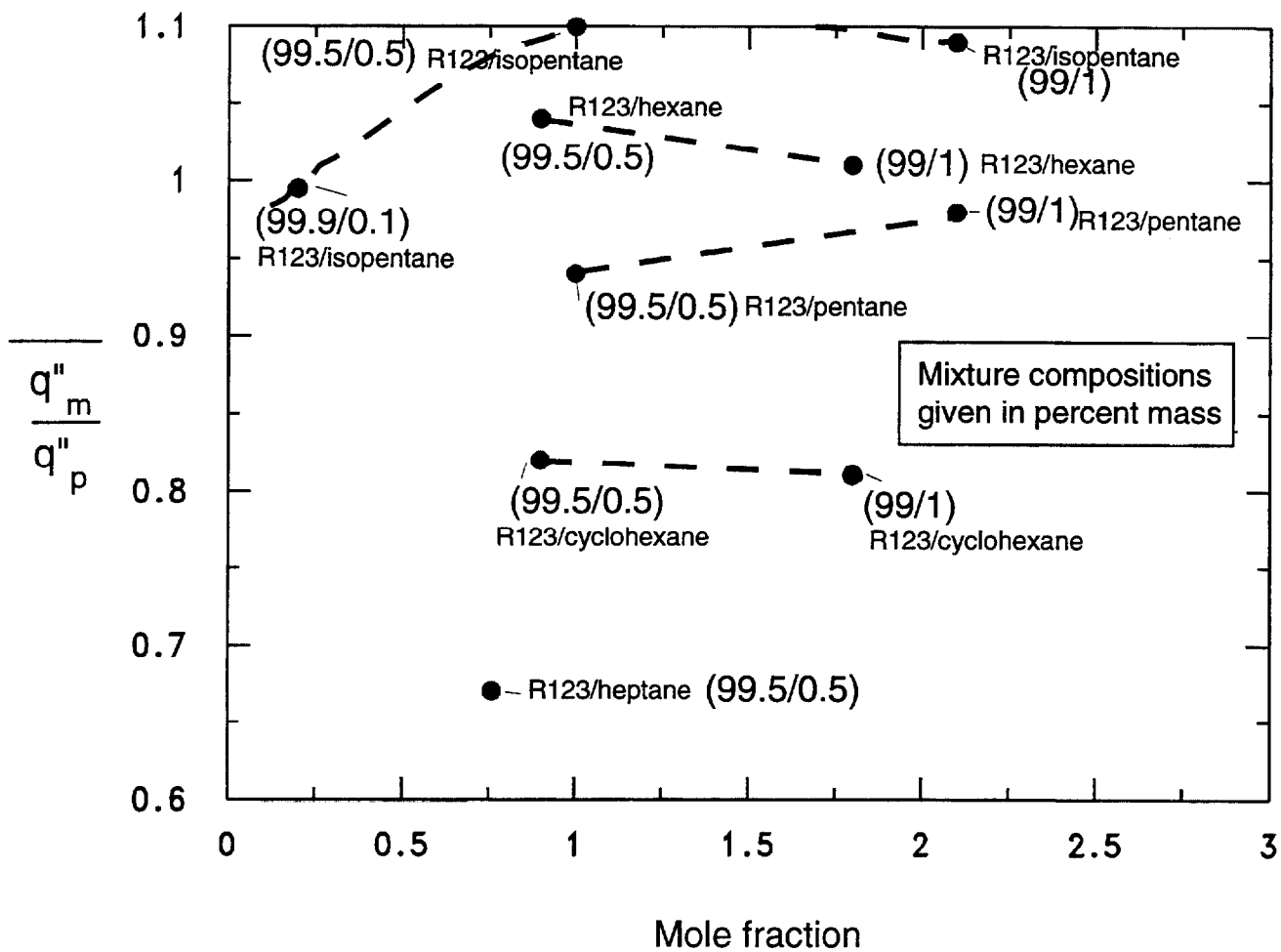


Fig. 25 Influence of mole fraction on the average enhancement ratio for dilute solutions of R123 and hydrocarbons

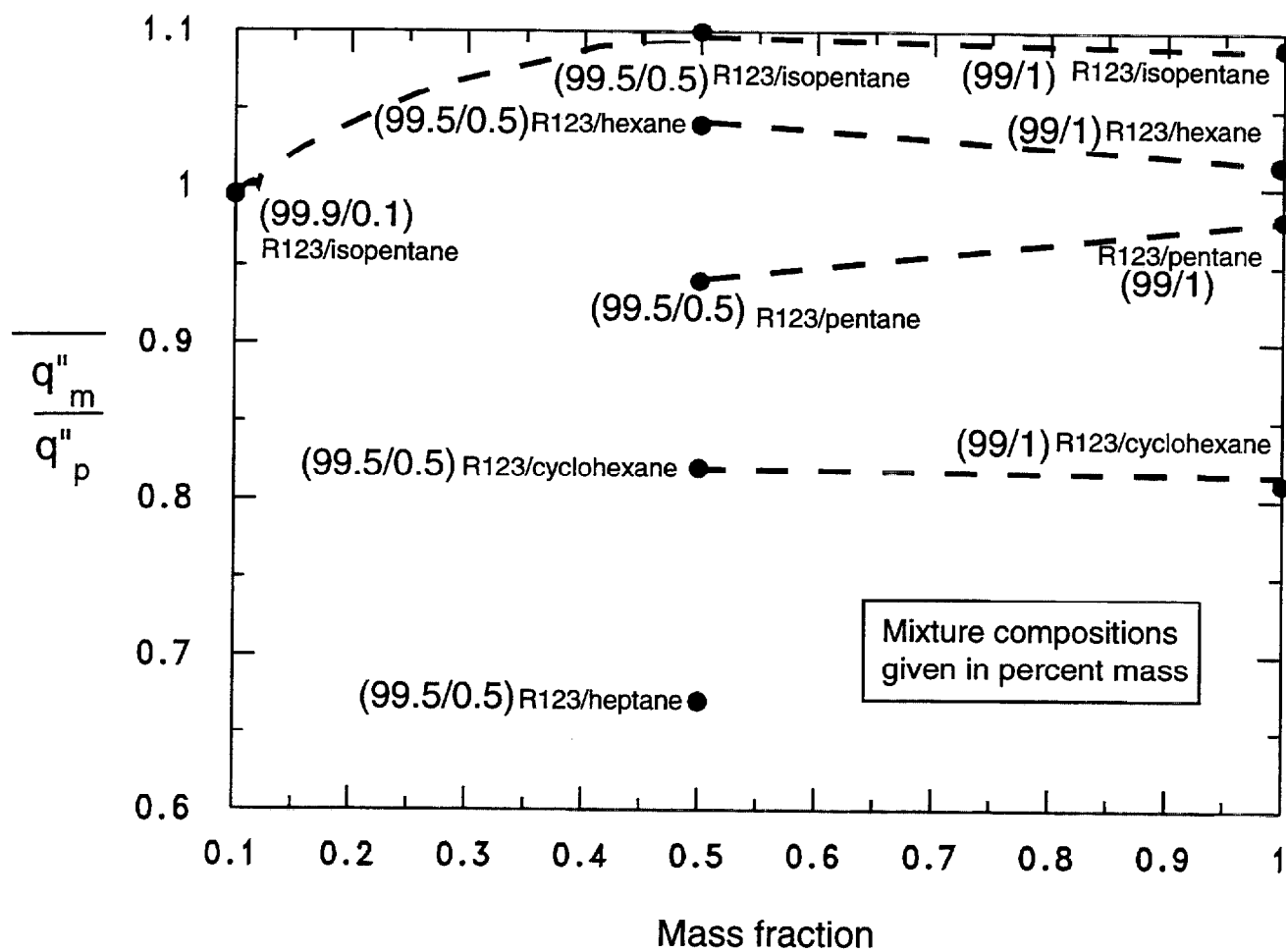


Fig. 26 Influence of mass fraction on the average enhancement ratio for dilute solutions of R123 and hydrocarbons